Title
THE ASYMMETRIC DEFORMATIONS OF MOLYBDENUM SINGLE CRYSTALS

Author
Lau, Silvanus Sui-Wai.

Publication Date
1969-06-01

UCRL-19013

cy. 2

THE ASYMMETRIC DEFORMATIONS OF MOLYBDENUM SINGLE CRYSTALS

Silvanus Sui-Wai Lau

PhD Thesis

June 1969

AEC Contract No. W-7405-eng-48

LAWRENCE RADIATION LABORATORY
UNIVERSITY of CALIFORNIA BERKELEY

UCRL-19013

cy. 2

DISCLAIMER

TABLE OF CONTENTS

THE ASYMMETRIC DEFORMATIONS OF MOLYBDENUM SINGLE CRYSTALS

Silvanus Sui-Wai Lau

Inorganic Materials Research Division, Lawrence Radiation Laboratory, Department of Materials Science and Engineering of the College of Engineering, University of California, Berkeley, California

ABSTRACT

The tensile properties of Mo single crystals of six different orientations were investigated over the range from 20°K to 550°K. The plastic behavior shows asymmetry in the critical resolved shear stress for slip on both {110} planes and {112}planes. At low temperatures, within the thermally activated region, slip seems to take place on well defined crystallographic planes. At high temperatures in this range, however, slip takes place on irrational planes. The asymmetries associated with yielding and slip both increase with decreasing temperature. These effects are rationalized in terms of a modified Peierls model. The model assumes the asymmetric slip arises from a tendency toward asymmetric splitting of the core of the a/2 ⟨111⟩ screw dislocation. It is shown that the model can predict with reasonable accuracy the stress-temperature-strain rate-orientation relationship and the slip behavior.

I. INTRODUCTION

In recent years the experimentally confirmed existance of several unique orientation effects on the plastic behavior of b.c.c. metals has added one more important factor to be considered in the already extremely complex and controversial problem of low temperature thermally activated deformation of b.c.c. metals.[1-11] In their review paper, Guyot and Dorn[12] have demonstrated the validity of the Peierls theory in rationalizing the thermally activated deformation of polycrystalline b.c.c. transition metals (W, Fe, Ta, Mo, Nb) and some alloys (AgMg, Fe-Si, etc.). In spite of this attractive feature of the Peierls theory, it cannot account for the asymmetries associated with yield strength and slip geometry in single crystals.

Since the pronounced presence of screw dislocations has been observed in Fe,[13] Mo,[14] Nb[15] and other b.c.c. metals and alloys[4] using transmission electron microscopy following low temperature deformation, the role of screw dislocations in the theories of thermally activated deformation has received much attention. Screw dislocations exhibit the unique possibility of lowering their energy by splitting so as to dissociate into partial dislocations lying in several slip planes coincident with their zone axis. This possibility in splitting and lowering of energy, and the observed facts of preferred screw orientation of dislocation after low temperature deformation, lead to the formulation of the current popular theories of thermally activated cross-slip of split screw dislocations.[1,2,3] The virtue of these theories is their capability to account for, at least qualitatively, the rapid increase of yield strength, the slip geometry and the asymmetry associated with yielding. The success of the models,

however, relies on the somewhat questionable special details in the assumed splitting of the dislocations. One major objection is the fact that in order to achieve even nominal agreement with the experimental facts, it must be assumed that the partial dislocation are separated from each other by at most one to two Burgers vectors. Under these conditions the partial dislocation cores overlap and the usual concepts of line energies, interaction energies and constriction energies for partial dislocations plus the concept of a stacking-fault energy are no longer valid. Thus, the very foundation on which these models have been erected are exposed as invalid. The deformation model based on the concept of elastic interactions between dislocations and tetragonal interstitial impurity strain centers also cannot account for the asymmetric behavior. Furthermore, it has been proven,[21,22,29] that interstitial impurities only alter the athermal stress levels of these b.c.c. crystals and do not significantly effect the thermal activation of dislocations.

Recently Dorn and Mukherjee[16] have formulated a modified Peierls model to rationalize the thermally activated deformation of b.c.c. metals. Their approach is based on a generalization of the Peierls mechanism which assumes an asymmetric dislocation core which is modified by the effective stress and permits cross slip. The theoretical predictions of this model seem to be in reasonable agreement with the limited data that are now available.

A. The Asymmetric Effects

In general, the asymmetric effects can be divided into three catagories. Each of these effects is closely related to the tensile orientation under investigation. These effects can be best described with the aid of the standard stereographic projection shown in Fig. 1. The angle χ_1', represents the angular rotation of the plane of maximum resolved shear stress from the $(\bar{1}01)$ plane. The angle ψ_1, represents the angular rotation of the observed slip plane and the angle λ_1, is the Schmid angle for slip in the [111] direction for the tensile orientation "+". Similar angular relationships hold for $[\bar{1}11]$ slip direction.

A schematic diagram of the expected ψ-χ' relations assuming crystal symmetry is given in Fig. 2 for exclusive operation of {101}, {211} or banal slip, (slip on the plane of maximum resolved shear stress). Sharp slip bands would be expected if only one kind of slip plane were operative. If symmetry prevailed and some cross slip took place the ψ-χ' curves would remain anti-symmetrical about $\chi'=0$ as shown by the broken curve of Fig. 2, and slip band would appear to be wavy except at $\chi'=-30°$, 0° and 30° where slip might be confined to lie almost exclusively on the $(\bar{1}\bar{1}2)$, $(\bar{1}01)$ and $(\bar{2}11)$ plane respectively.

The asymmetric effects are summarized as follows: (1) Asymmetry of yielding: As demonstrated in Fig. 3a and b, the yield strength of the crystal changes asymmetrically as the tensile orientation changes. The dotted line represents the symmetrical change as depicted by Schmid Law. A detailed investigation on asymmetric yield in Fe-2.7 Si alloy was reported by Taoka, Takeuchi and Furubayashi.[4] Similar trends have been observed on Nb,[15] Mo,[5] Ta, Nb and Mo[6] and other b.c.c. metals.

(2) Asymmetry of slip: Figures 3c and 3d show schematically the asymmetric ψ_1 X_1', curves for Fe-Si alloys,[1,4,7,8] as compared with the symmetric ψ_1 X_1', curves show in Fig. 2. If slip geometry was governed by crystal symmetry, operative slip planes for orientations with positive X', should be related to those with negative X', by a symmetry operation. It is evident from Fig. 3c and d that such a symmetry operation fails to relate the ψ_1-X_1' curve from positive X_1' to negative X_1'. ψ_1-X_1' curves of this kind are typical of the asymmetric slip of b.c.c. metals at low temperatures. As the temperature increases, the observed asymmetry reduces accordingly. (3) Asymmetry of stressing direction: When the sign of the stress changes from tension to compression, the asymmetries for yielding and slip geometry are inverted as shown schematically in Figs. 3a, b, c, d. This asymmetric effect has been reported by Taoka et al,[4] Sestak and Zarubova,[7] and other investigators on Fe-Si alloys.

Similar inversion of yield strength upon the change of sign of stress is reported by Sherwood et al.,[6] on Ta, Nb and Mo. It is suggested that the equivalence of $(\bar{2}11)$ [111] with $(\bar{1}\bar{1}2)[\bar{1}\bar{1}\bar{1}]$ difficult slip and the equivalence of $(\bar{1}\bar{1}2)[111]$ with $(\bar{2}11)[\bar{1}\bar{1}\bar{1}]$ easy slip lead to the inversion. This suggests that when atoms move in the twinning direction, (in a dislocation reaction on {112}plane of the type:

$$1/2\ \langle 111\rangle = 1/6\ \langle 111\rangle + 1/3\ \langle 111\rangle,$$

the twinning direction is the direction where the resolved shear stress would make the twinning partial 1/6 ⟨111⟩ to glide first, the antitwinning direction is the direction where the resolved shear stress would make the complementary partial 1/3 ⟨111⟩ to glide first), slip is easy, e.g. [111] slip on the $(\bar{1}\bar{1}2)$ plane under tension, and when atoms move in the antitwinning direction, slip becomes difficult, e.g.[111] slip on

($\bar{2}11$) plane under tension. All three types of asymmetries increase with decreasing temperature, and all seem to be closely related to the atomic movement in either the twinning or antitwinning direction. Because of these common features of the asymmetries, it is strongly suspected that they have a common origin.

The major objective of this investigation was to establish experimentally the effect of orientation and test temperature on the asymmetric yielding and slip band formation under tensile straining of single crystals. Molybdenum was selected for this investigation because it was known to exhibit high asymmetries than Nb, Fe and Fe-Si alloys. A second objective was to test the accuracy of the recently announced modified Peierls mechanism. In order to permit definitive correlations between theory and experiment, special orientations were selected for study.

II. EXPERIMENTAL PROCEDURE

Molybdenum rods (1/4 in. diameter, commercially pure) were purified by the electron beam zone refining technique. Oriented single crystals are grown with four molten zone passes. These crystals were machined into specimens of the following dimensions: total length 1.5 in., gage length 0.8 in., square cross section of 0.125 in. × 0.125 in. The shoulders at both ends were threaded and the shoulder radius is 0.125 in. (Fig. 4). Electropolishing in H_2SO_4-CH_3OH solution was used to remove the surface mechanical damage on the specimens. The polishing equipment consisted of a rotating stage where eight specimens could be polished at the same time. The specimens were first attached to the stage in a vertical position. The stage was then lowered into the polishing solution. The rotation speed of the stage was approximately 1 cycle/min. The specimen position was reversed every 15 minutes of polishing time to ensure dimensional uniformity. After approximately one hour of polishing, the x-ray Laue patterns of the surfaces indicate that all observable surface mechanical damage was removed. These specimens were then annealed in an ultra-pure He atmosphere for 24 hours at 2000°C, to achieve a standard initial state for all the test specimens. The interstitial impurity concentration of the specimens showed by the vacuum fusion method: C(.009 wt.%), O(.002 wt.%), and N(.001 wt.%). Resistivity ratio: $\frac{\rho_{273°K}}{\rho_{4.2°K}} \approx 10^3$. The annealed specimens were electropolished again for 2-3 minutes. Specimens were found to be very brittle after annealing without electropolishing (Stein reported the same phenomenon[5]). The variations of the width and thickness were not more than .002 in., the specimen

surface was shiny, smooth and good for slip line observation. The specimens were tested in tension (nominal strain rate = 3.3×10^{-5} sec^{-1}) at different temperatures and to various strains. The yield stress was measured at 0.2% plastic strain. The slip lines were observed using the Normarski interference contrast technique. Operative slip systems were determined by the two surface trace analysis method.

III. EXPERIMENTAL RESULTS

Six orientations within the standard stereographic triangle were investigated (as shown in Fig. 5). Both [111] and [$\bar{1}$11] directions have been identified in the literature.[3,8,9,17,18] Each orientation was identified in term of λ_1, χ'_1, and λ_2, χ'_2 as shown in Table I.

General observation of the mechanical data for tension indicates a strong temperature dependence of yield strength. This temperature dependence varies, however, with respect to tensile orientation, i.e. stronger in tension for orientations near the [111] - [011] boundary and weaker for those near [001]. At high temperatures ($\approx$550°K), slip lines were observed with optical microscope to be coarse, wavy and crystallographic. At intermediate temperatures ($\approx$350°K), slip lines were finer and less wavy, slip seems to take place on irrational planes. At low temperatures ($\approx$77°K), slip lines were very fine and straight, slip traces fall on low indexed planes. The temperature normal yield stress relationship for different orientations is shown in Fig. 6. The plastic behavior is summarized in the following tables shown on pages 11-14.

Slip traces can be detected at strains as low as .04% with the aid of the Normarski interference contrast technique (resolution limit $\approx 3\times10^{-4}$ cm.) At this low strain, usually only one operative slip plane is detected near the center of the specimen. Near the shoulders at both ends, more complex slip traces are observed even at the very beginning of plastic flow. This is due to the shoulder radius effects which give rise to a more complex stress state at the ends than that near the center which is under simple tension stress. At higher strains, other slip traces are detectable throughout the specimen. The optical microscope observable on-set strain

of new slip traces depends primarily on temperature and tensile orientation. At 550°K and of tensile orientations most favorable for only one operative slip system, (i.e. orientation B), the strain for the observed on-set of slip traces other than the primary slip is 2% or more. This on-set strain decreases with decreasing temperature. Also as the tensile orientation changes to a more favorable area within the standard triangle for multiple slip, slip traces become very complex (three systems or more) at intermediate strains, this again depends on temperature and orientation, (i.e., "B," 1%, 300°K) faint and unidentifiable traces are, sometimes, observed. As the plastic strain increases to more than a few percent, the slip behavior "simplifies", usually only one or two highly stressed systems remain. One of the remaining systems at high strain is usually the one observed at very low strain. Similar slip behavior was noted in Mo-10 at.% Re alloy.[19] A comparison of results of slip behavior reported here with those very limited results reported recently in the literature[17,18,20] indicates a general agreement on the choice of slip systems. The details of slip behavior, however, vary from one investigator to another, i.e. the on-set of secondary slips, the prevalence of certain systems at a certain temperature, strain and orientation, etc. The differences in the details of slip behavior can be attributed to methods of investigation, specimen end or stress concentration effects, specimen size effect and purity of specimen etc.

The yield strengths of the crystals vary vastly with temperature (as shown in Fig. 6). The stress-temperature curves for $X > 0$ lie above that for $X'=0$, and those for $X'<0$ lie below. The difference in these curves is more pronounced for $X'>0$ and at low temperatures. Part of the difference is due to the difference in the Schmid angle λ, and the rest due to the asymmetric effects. If the Schmid angle for each orientation

were normalized to that for $\chi_1' = 0$ ($\lambda = 54°$), the difference in the stress-temperature curve, is, then primarily due to the asymmetries, (Fig. 7). Observations on the mechanical data and slip behavior indicate that larger asymmetric effects are associated with {110} slip planes than those with {112} slip planes at low temperatures, (Figs. 6, 7 and 15). Between 300°K to 450°K, slip is less rational, and the asymmetries reduce. One special feature worth mentioning is the fact that rational $(\bar{2}11)$ slip is never observed at small plastic strains [$(\bar{2}11)$ slip plane is only observed at 158°K, 13.6% elongation for orientation A]. Even for orientation "C" where the $(\bar{2}11)$ plane is most highly stressed, only $(\bar{1}01)$ and $(\bar{1}10)$ slip planes are observed. Even at the critical temperature where slip usually takes on the rational plane with the highest Schmid factor, heavy cross slips between $(\bar{1}10)$ and $(\bar{1}01)$ planes were observed giving a pseudo $(\bar{2}11)$ slip plane (Fig. 10e). This reveals that the $(\bar{2}11)$ plane has an usually high critical stress for slip in tension.

The athermal stress level $\sigma_{550°K}$ depends primarily on the impurity concentrations, the dislocation density and arrangement.[10,21,22] This stress level for all annealed specimens varies between 1 to $2\times10^{+8}$ dynes cm^2, suggesting that the conditions (impurity, dislocation, etc.) of all specimens are quite the same and the stress level is small compared with those at lower temperatures. The critical temperatures (the temperature at which the thermally activated stress first becomes zero; $\sigma^*_{Tc} = 0$) for all orientations appear to be identical and equal to 450°K.

TABLE I

Orientation	λ_1: The Schmid Angle for slip in the [111] direction	χ_1: The angle between the plane of max. shear stress and $(\bar{1}01)$	λ_2= The Schmid angle for slip in the $[\bar{1}11]$ direction	χ'_2= The angle between the plane of max. shear stress and (101)
A	55.5°	-16°	43°	-30°
B	54°	0°	30°	-21°
C	64°	+28°	6°	+15°
D	44°	+16°	29°	+10°
E	45.5°	- 6°	39°	-13°
G	42°	- 4°	39°	- 5°

TABLE II Orientation A

T°K	$\sigma^*_{.2\%} = \left(\sigma_T - \sigma_{550°K}\right) \pm 0.2 \times 10 \frac{8 \text{ dynes}}{cm^2}$	Observed Slip traces: ψ_2 ±2°(Fig. 8)
0	71.5 (extrapolated value)	
55	50.9	
77	42.5	-30°
156	27.1	-30°
298	13.1	-32°
375	7.9	-34°
425	1.1	
550	0	-30°

TABLE III Orientation B

T°K	$\sigma^*_{.2\%} = \left(\sigma_T - \sigma_{550°K}\right) \pm 0.2 \times 10 \frac{8 \text{ dynes}}{cm^2}$	Observed Slip traces: $\psi_1 \pm 2°$ (Fig. 9)
0	94.5 (extrapolated value)	
25	76.6	
52	65.5	
77	56.5	0° (77°K)
153	40.7	
196	33.1	
296	18.6	0° (298°K)
425	1.28	0° (325°K), 0° (356°K)
550	0	0° (550°K)

TABLE III Orientation C

T°K	$\sigma^*_{.2\%} \pm .2\times10 \frac{8 \text{ dynes}}{\text{cm}^2}$	Observed slip traces: $\psi_1 \pm 2°$ (Fig. 10)
0	190.0 (extrapolated value)	
20	156.0	
41	127.0	
77	80.7	0°
160	52.0	0°
298	22.0	+6°
350	10.2	+15°
400	4.1	
453	0	heavy $(\bar{1}01)$, $(\bar{1}10)$ cross slip

TABLE IV Orientation D

T°K	$\sigma^*_{.2\%} \pm .2\times10 \frac{8 \text{ dynes}}{\text{cm}^2}$	Observed slip traces: $\psi_1 \pm 2°$ (Fig. 11)
0	117.5 (extrapolated value)	
27	102.0	
77	74.7	0°
159	51.5	0°
301	21.8	0°
351	10.2	0°
400	2.15	
550	0	$(\bar{1}01)$, $(\bar{1}\bar{1}2)$ cross slip

TABLE V Orientation E

T	$\sigma^*_{.2\%} \pm .2\times10^8 \frac{\text{dynes}}{\text{cm}^2}$	Observed slip traces ±2° (Fig. 12)
0	79.0 (extrapolated value)	
20	68.6	
77	47.3	$\psi_2 = 30°$
153	29.3	$\psi_1 = -6°$, $\psi_2 = -24°$
298	15.1	$\psi_2 = -20°$
352	9.34	$\psi_1 = -10°$, $\psi_2 = -12°$
550	0	$\psi_1 = 0°$, $\psi_2 = 0°$

TABLE VI Orientation G

T	$\sigma^*_{.2\%} \pm .2\times10^8 \frac{\text{dynes}}{\text{cm}^2}$	Observed slip traces (±2°) (Fig. 13)
0	85.0 (extrapolated value)	
33	71.7	
50	61.3	
77	46.2	$\psi_1 = 0°$, $\psi_2 = 0°$
159	24.8	
298	14.8	$\psi_1 = -5°$, $\psi_2 = -5°$
350	9.2	$\psi_1 = -8°$, $\psi_2 = -8°$
550	0	$\psi_1 = 0°$

IV. DATA ANALYSIS

The unique plastic behavior of Mo single crystals has been described in the previous sections. It is the objective of this section to analyze these data, rationalize the data in terms of a dislocation model and attempt to make some generalization. A successful dislocation model for plastic deformation of b.c.c. metals must have the ability to explain (1) the strong temperature dependence of yield stress, (2) the asymmetries associated with yielding, and (3) slip geometry. The model, above all, must also have sound physical foundation and must be self-consistant. The thermally activated cross slip of dissociated partial dislocations[1-3] is a currently popular model. It has been applied to the deformation of Nb[9,13] and Fe-Si[1] alloy with qualitative and partial quantitative success. As mentioned in Section I, the model relies on the dissociation geometry of the screw dislocation and on the concept of cross slipping of these narrowly dissociated partials whose cores are overlapped. In addition to these objections, the cross slip model predicts a somewhat stronger temperature dependence of yield stress in the low temperature region than indicated by experimental results. Furthermore, Vitek[24] has shown recently that no stable intrinsic stacking faults can exist either on {110} planes or {112} planes in b.c.c. crystals. The dissociation geometry of partial dislocations on {110} and {112} planes, therefore, cannot have a realistic and meaningful foundation. Vitek further suggests that a more realistic splitting of the screw dislocation represents a model of the dissociated core.

Dorn and Mukherjee[1] have recently introduced the dissociated core concept to the line energy model of the Peierls theory[25] to rationalize

the thermally activated deformation of b.c.c. metals. This modified Peierls theory has been applied to the limited data now available in literature and appears to enjoy reasonable success. The experimental results of the present investigation will be rationalized in terms of this modified model to provide a critical test for its validity under more extensive conditions than heretofore available.

A. The Modified Peierls Model

The modified Peierls model assumes that the thermally activated deformation of b.c.c. metals is controlled by thermally assisted formation of kink pairs on screw dislocations. The core of the screw dislocation is assumed to be split, i.e. the atoms in the core tend to lower the core energy of the dislocation by readjusting their positions. Under an applied stress, the core becomes asymmetric (Figs. 14 a and b). When the screw dislocation is activated it moves from one row of atoms to another and the core atoms take a more planar configuration on the slip plane. Therefore, there is an increase in energy. This "activated" screw dislocation forms a pair of kinks and moves out of the "Peierls" valley by one atomic spacing under the action of the applied stress. It is assumed that the screw dislocation is again split to lower its energy after the screw dislocation has moved one atomic spacing. When the next thermal activation comes, it may or may not slip on the same slip plane as it did previously. The probability that the screw dislocation will cross slip to other possible slip planes depends on the temperature and the relative magnitude of the activation energies on all different slip planes. The magnitude of the activation energies, in turn, depends on the stress, the orientation and the asymmetry of the core. Therefore,

screw dislocations in general slip on the plane or intimately (on an atomic scale) cross slip between planes having the lowest activation energies. Since the asymmetry of the cores perturbsthe Peierls stresses on different possible slip planes which, in turn, change the activation energies on different possible slip planes, the yielding and the slip behavior of the crystal must conform with the asymmetry of cores and become asymmetric.

The mathematical formulation of the model is presented briefly here. According to the Dorn-Rajnak[24] approach to the Peierls Process, the kink energy, U_k, can be approximated by

$$U_k = \frac{2\Gamma a}{\pi}\left(\frac{2\tau_p ab}{\pi\Gamma}\right)^{1/2} \qquad (1)$$

where $\Gamma \simeq 1/2\ Gb^2$ is the dislocation line energy, G is the shear modulus of elasticity, a is the spacing between the Peierls valleys, b is the Burgers vector and τ_p is the Peierls stress. The energy, Un, that needs to be supplied by a thermal fluctuation in order to nucleate a pair of kinks will be approximated by

$$Un = 2U_k\ f\left\{\frac{\tau^*}{\tau_p}\right\} \simeq \frac{4\Gamma a}{\pi}\left(\frac{2\tau_p ab}{\pi\Gamma}\right)^{1/2}\left(1 - \frac{\tau^*}{\tau_p}\right)^{3/2} \qquad (2)$$

where τ^* is the effective resolved shear stress on the slip plane. The stress dependence of Un also varies as the shape of the Peierls changes.[2] While Eq. (2) describes a sinusoidal Peierls hill, the quasiparabolic hill can be approximated by

$$Un = \pi a\sqrt{\frac{ab\tau_p\Gamma}{8}}\left(1 - \frac{\tau^*}{\tau_p}\right)^2 \qquad (3)$$

Although the hill shape of a split screw dislocation is not known, it seems appropriate that the hill shape resembles the quasiparabolic model. Because of empirical reasons that it gives better experimental fit, the stress dependence of Un for Mo single crystal is taken as 1.85 which is not too much different from that for a quasiparabolic hill.

The following assumptions were made: (1) As mentioned above, the thermally-activated deformation of b.c.c. metals is controlled by thermally-assisted formation of kink pair on screw dislocations. (2) For tensile or compression axes within the standard stereographic triangle only the 1/2 [111] and 1/2 [$\bar{1}$11] screw dislocations become activatable. This arises because the resolved shear stress is too low to induce activation of other screw dislocations. (3) Slip can take place only on planes of the form {101} and {112} that belong to the [111] and [$\bar{1}$11] zone axes. The theory can easily be modified to include slip on planes of other forms, e.g.{123}, if and when definitive evidence for the operation of such slip planes is obtained. (4) Cross slip of the 1/2 [111] screw dislocations is assumed to take place between the ($\bar{1}$10), ($\bar{2}$11), ($\bar{1}$01), ($\bar{1}\bar{1}$2) and (0$\bar{1}$1) planes. The specimen orientation is given by λ_1 and χ_1' shown in Fig. 1. (5) Cross slip of the 1/2 [$\bar{1}$11] screw dislocation is assumed to take place between (110), (211), (101), (1$\bar{1}$2), and (0$\bar{1}$1) planes. The specimen orientation relative to these slips is designed by λ_2 and χ_2'. λ_2 and χ_2' are not independent variables since they are related to λ_1 and χ_1' by $\lambda_2 = \lambda_2\{\lambda_1, \chi_1'\}$ and $\chi_2' = \chi_2'\{\lambda_1, \chi_1'\}$

When an effective tensile stress σ^* is applied in the direction of λ_1, χ_1' and λ_2, χ_2', the effective resolved shear stresses on the assumed slip planes are given by

$$\tau^*_{\bar{1}10} = \sigma^* \cos\lambda_1 \sin\lambda_2 \cos(60-\chi_1') \quad (4a)$$

$$\tau^*_{\bar{2}11} = \sigma^* \cos\lambda_1 \sin\lambda_1 \cos(30-\chi_1') \quad (4b)$$

$$\tau^*_{\bar{1}01} = \sigma^* \cos\lambda_1 \sin\lambda_1 \cos\chi_1' \quad (4c)$$

$$\tau^*_{\bar{1}12} = \sigma^* \cos\lambda_1 \sin\lambda_1 \cos(30+\chi_1') \quad (4d)$$

$$\tau^*_{0\bar{1}1} = \sigma^* \cos\lambda_1 \sin\lambda_1 \cos(60+\chi_1') \quad (4e)$$

$$\tau^*_{0\bar{1}1} = \sigma^* \cos\lambda_2 \sin\lambda_2 \cos(60+\chi_2') \quad (5a)$$

$$\tau^*_{1\bar{1}2} = \sigma^* \cos\lambda_2 \sin\lambda_2 \cos(30+\chi_2') \quad (5b)$$

$$\tau^*_{101} = \sigma^* \cos\lambda_2 \sin\lambda_2 \cos\chi_2' \quad (5c)$$

$$\tau^*_{211} = \sigma^* \cos\lambda_2 \sin\lambda_2 \cos(30-\chi_2') \quad (5d)$$

$$\tau^*_{110} = \sigma^* \cos\lambda_2 \sin\lambda_2 \cos(60-\chi_2) \quad (5e)$$

The asymmetry of the Peierls stress is based on the concept that the asymmetrical arrangement of the atoms in the core of the dislocation is perturbed by the applied stress. To a first approximation the perturbation is expected to be linear with the resolved shear stress. The asymmetric Peierls stresses are represented by

$$\tau_{p\bar{1}10} = P_{\bar{1}01} + A_{\bar{1}01}\,\sigma^* \cos\lambda_1 \sin\lambda_1 \sin 3\chi_1' \quad (6a)$$

$$\tau_{p\bar{2}11} = P_{\bar{2}11} + A_{\bar{2}11}\,\sigma^* \cos\lambda_1 \sin\lambda_1 \sin 3\chi_1' \quad (6b)$$

$$\tau_{p\bar{1}01} = P_{\bar{1}01} + A_{\bar{1}01}\,\sigma^* \cos\lambda_1 \sin\lambda_1 \sin 3\chi_1' \quad (6c)$$

$$\tau_{p\bar{1}\bar{1}2} = P_{\bar{1}\bar{1}2} + A_{\bar{1}\bar{1}2}\,\sigma^* \cos\lambda_1 \sin\lambda_1 \sin 3\chi_1' \quad (6d)$$

$$\tau_{p0\bar{1}1} = P_{\bar{1}01} + A_{\bar{1}01}\,\sigma^* \cos\lambda_1 \sin\lambda_1 \sin 3\chi_1' \quad (6e)$$

$$\tau_{p0\bar{1}1} = P_{\bar{1}01} + A_{\bar{1}01}\,\sigma^* \cos\lambda_2 \sin\lambda_2 \sin 3\chi_2' \quad (7a)$$

$$\tau_{p1\bar{1}2} = P_{\bar{1}\bar{1}2} + A_{\bar{1}\bar{1}2}\,\sigma^* \cos\lambda_2 \sin\lambda_2 \sin 3\chi_2' \quad (7b)$$

$$\tau_{p101} = P_{\bar{1}01} + A_{\bar{1}01}\,\sigma^* \cos\lambda_2 \sin\lambda_2 \sin 3\chi_2' \quad (7c)$$

$$\tau_{p211} = P_{\bar{2}11} + A_{\bar{2}11}\,\sigma^* \cos\lambda_2 \sin\lambda_2 \sin 3\chi_2' \quad (7d)$$

$$\tau_{p110} = P_{\bar{1}01} + A_{\bar{1}01}\,\sigma^* \cos\lambda_2 \sin\lambda_2 \sin 3\chi_2' \quad (7e)$$

The component of the Peierls stress $P_{hk\ell}$ is the true Peierls stress of the $(hk\ell)$ plane when no stress is applied. $P_{\bar{2}11}$, obtained when the atoms are moved in the antitwinning direction, might be expected to exceed $P_{\bar{1}\bar{1}2}$ which applied when the atom motion is in the twinning direction. On the other hand, $P_{\bar{1}01}$ is expected to be the same for all planes of the form $(\bar{1}01)$ as assumed in Eqs. (6) and (7). The A's represent asymmetry factors that account for modifications of the Peierls stress due to atomic displacements in the dislocation core as a result of the applied stress. The asymmetric effects are further assumed to depend on $\sin 3X'$ as suggested by the three-fold symmetry axis which should apply to screw dislocations in the $\langle 11\bar{1}\rangle$ directions. For positive values of X', the applied stress causes the core to split more on $(\bar{1}\bar{1}2)$ and $(1\bar{2}1)$ planes because the stress is in the twinning directions on these planes, and less on the $(\bar{2}11)$ plane because the stress is in the antitwinning direction (Fig. 14). The perturbation, therefore, moves the atoms toward a more difficultly activated arrangement. For negative values of X', the applied stress causes the core to extend more on $(\bar{1}\bar{1}2)$ because of twinning direction, whereas, atoms on $(\bar{2}11)$ and $(1\bar{2}1)$ are constricted to a lesser degree toward the center because of antitwinning consideration. This perturbation makes activation easier on either $(\bar{1}01)$ or $(\bar{1}\bar{1}2)$ or both. Upon the inversion of stress, the reverse holds.

The frequency of activation for cross slip of the 1/2 [111] screw dislocation is independent of that of 1/2 $[\bar{1}11]$ screw dislocation. On the other hand, the frequency of activation of either of these dislocations on one of the possible cross slip planes of the same zone is mutually exclusive of cross slip on any other of the possible cross slip planes per anyone event. Consequently the actual frequencies of

activation for cross slip on the (hkℓ) plane are given by

$$\nu^{*}_{hk\ell[111]} = \left(\frac{\nu^{2}_{hk\ell}}{\nu_{110} + \nu_{211} + \nu_{101} + \nu_{112} + \nu_{011}} \right)_{[111]} \qquad (8a)$$

$$\nu^{*}_{hk\ell[\bar{1}11]} = \left(\frac{\nu^{2}_{hk\ell}}{\nu_{0\bar{1}1} + \nu_{1\bar{1}2} + \nu_{101} + 211 + \nu_{110}} \right)_{[\bar{1}11]} \qquad (8b)$$

where

$$\nu_{hk\ell[111]} = \left(\frac{\nu_0 L_1 b^2 \tau_{phk\ell 1}}{\pi^2 a_{hk\ell}\, \Gamma} \quad e^{-U_{hk\ell 1}/kT} \right) \text{ (frequency} \qquad (9a)$$

of activation on a single (hkℓ) plane of [111] zone)

$$\nu_{hk\ell[\bar{1}11]} = \left(\frac{\nu_0 L_{\bar{1}} b^2 \tau_{phk\ell\bar{1}}}{\pi^2 a_{hk\ell}\, \Gamma} \quad e^{-U_{hk\ell\bar{1}}/kT} \right) \text{ (frequency of} \qquad (9b)$$

activation on a single (hkℓ) plane of [111] zone),

where ν_0 is the Debye frequency, L is the average length of a dislocation that might be swept out by a pair of kinks following their nucleation, Γ is the dislocation line energy, $a_{hk\ell}$ is the distance between parallel rows of atoms on the (hkℓ) plane and kT has its usual meaning of the Boltzmann constant times the absolute temperature. The shear strain rates on any plane of the two designated zones are given by

$$\dot{\epsilon}_{hk\ell_1} = \rho_1 b\, a_{hk\ell}\, \nu^{*}_{hk\ell_1} \qquad (10a)$$

$$\dot{\epsilon}_{hk\ell_{\bar{1}}} = \rho_{\bar{1}} b\, a_{hk\ell}\, \nu^{*}_{hk\ell_1} \qquad (10b)$$

where ρ_1 and $\rho_{\bar{1}}$ refer to the densities of the screw dislocations in these zones. In summary the total tensile strain rate, $\dot{\epsilon}$, obtained the

tensor summation of all shear strain rate is given by

$$\dot{\epsilon} = \cos\lambda_1 \sin\lambda_1 \{\dot{\epsilon}_{\bar{1}101}\cos(60-\chi_1') + \dot{\epsilon}_{\bar{2}111}\cos(30-\chi_1') + \dot{\epsilon}_{\bar{1}011}\cos\chi_1' + \dot{\epsilon}_{\bar{1}\bar{1}21}\cos(30+\chi_1') + \dot{\epsilon}_{0\bar{1}11}\cos(60+\chi_1')\} + \cos\lambda_2 \sin\lambda_2 \{\dot{\epsilon}_{0\bar{1}1\bar{1}}\cos(60+\chi_2') + \dot{\epsilon}_{1\bar{1}2\bar{1}}\cos(30+\chi_2') + \dot{\epsilon}_{101\bar{1}}\cos\chi_2' + \dot{\epsilon}_{211\bar{1}}\cos(30-\chi_2')\} \tag{11}$$

The angles ψ_1 and ψ_2 that slip bands for [111] and [$\bar{1}$11] zones make with the ($\bar{1}$01) and the (101) planes respectively are established by vector addition to be

$$\cot\psi_1 = \frac{\frac{1}{2}\nu^*_{\bar{1}10}a_{\bar{1}10} + \frac{\sqrt{3}}{2}\nu^*_{\bar{2}11}a_{\bar{2}11} + \nu^*_{\bar{1}01}a_{\bar{1}01} + \frac{\sqrt{3}}{2}\nu^*_{\bar{1}\bar{1}2}a_{\bar{1}\bar{1}2} + \frac{1}{2}\nu^*_{0\bar{1}1}a_{0\bar{1}1}}{\frac{\sqrt{3}}{2}\nu^*_{\bar{1}10}a_{\bar{1}10} + \frac{1}{2}\nu^*_{\bar{2}11} - \frac{1}{2}\nu^*_{\bar{1}\bar{1}2}a_{\bar{1}\bar{1}2} - \frac{\sqrt{3}}{2}\nu^*_{0\bar{1}1}a_{0\bar{1}1}} \tag{12a}$$

$$\cot\psi_2 = \frac{\frac{1}{2}\nu^*_{0\bar{1}1}a_{0\bar{1}1} + \frac{\sqrt{3}}{2}\nu^*_{1\bar{1}2}a_{1\bar{1}2} + \nu^*_{101}a_{101} + \frac{\sqrt{3}}{2}\nu^*_{211}a_{211} + \frac{1}{2}\nu^*_{110}a_{110}}{\frac{\sqrt{3}}{2}\nu^*_{0\bar{1}1}a_{0\bar{1}1} - \frac{1}{2}\nu^*_{1\bar{1}2}a_{1\bar{1}2} + \frac{1}{2}\nu^*_{211}a_{211} + \frac{\sqrt{3}}{2}\nu^*_{110}a_{110}} \tag{12b}$$

B. Method of Analysis

Since there are ten terms in the strain rate equation and each term has a different exponential term, this makes the calculation of yield stress-temperature relationship for a given strain rate a rather complicated manipulation. Fortunately we can take advantage of the fast speed of the CDC 6600 computer and sometimes the analysis can be guided by the experimental slip traces.

In order to simplify the calculation, we will write the following equations: for $X' = 0$, the "true" Peierls stress on $(\bar{1}01)$ plane is represented by

$$P_{\bar{1}01} = \sigma^*_{0,0} \cos \lambda_1 \sin \lambda_1 \tag{13}$$

where $\sigma^*_{0,0}$ is the effective stress for $X' = 0$ at 0°K, and λ_1 is the Schmid angle for $[\bar{1}11]$ direction. The "true" Peierls stresses on $(\bar{1}\bar{1}2)$ plane and $(\bar{2}11)$ plane are represented by

$$P_{\bar{1}\bar{1}2} = \alpha_1 \sigma^*_{0,0} \cos \lambda_1 \sin \lambda_1 \tag{14}$$

$$P_{\bar{2}11} = \alpha_2 \sigma^*_{0,0} \cos \lambda_1 \sin \lambda_1 \tag{15}$$

respectively. Where α_1 and α_2 are positive constants that may be either greater than or less than unity. We further assume that

$$P_{(211)[\bar{1}11]} = P_{(\bar{2}11)[111]} \tag{16}$$

and

$$P_{(\bar{1}\bar{1}2)[111]} = P_{(1\bar{1}2)[\bar{1}11]} \tag{17}$$

because of crystallographic equivalence in antitwinning and twinning direction, respectively. With this simplfication, we can write the following equations:

$$\tau_{p\bar{1}10} = \sigma^{*}_{0,0} \cos\lambda_1 \sin\lambda_1 + A_{\bar{1}01}\, \sigma_{T,\chi_1'} \cos\lambda_1 \sin\lambda_1 \sin 3\chi_1' \qquad (18a)$$

$$\tau_{p\bar{2}11} = \alpha_2\sigma^{*}_{0,0} \cos\lambda_1 \sin\lambda_1 + A_{\bar{2}11}\sigma_{T,\chi_1'} \cos\lambda_1 \sin\lambda_1 \sin 3\chi_1' \qquad (18b)$$

$$\tau_{p\bar{1}01} = \sigma^{*}_{0,0} \cos\lambda_1 \sin\lambda_1 + A_{\bar{1}01}\, \sigma^{*}_{T,\chi_1'} \cos\lambda_1 \sin\lambda_1 \sin 3\chi_1' \qquad (18c)$$

$$\tau_{p\bar{1}\bar{1}2} = \alpha_1\sigma^{*}_{0,0} \cos\lambda_1 \sin\lambda_1 + A_{\bar{1}\bar{1}2}\, \sigma^{*}_{T,\chi_1'} \cos\lambda_1 \sin\lambda_1 \sin 3\chi_1' \qquad (18d)$$

$$\tau_{p011} = \sigma^{*}_{0,0} \cos\lambda_1 \sin\lambda_1 + A_{\bar{1}01}\, \sigma^{*}_{T,\chi_1'} \cos\lambda_1 \sin\lambda_1 \sin 3\chi_1' \qquad (18e)$$

$$\tau_{p0\bar{1}1} = \sigma^{*}_{0,0} \cos\lambda_1 \sin\lambda_1 + A_{\bar{1}01}\, \sigma^{*}_{T,\chi_2'} \cos\lambda_2 \sin\lambda_2 \sin 3\chi_2' \qquad (19a)$$

$$\tau_{p1\bar{1}2} = \alpha_1\sigma^{*}_{0,0} \cos\lambda_1 \sin\lambda_1 + A_{\bar{1}\bar{1}2}\sigma^{*}_{T,\chi_2'} \cos\lambda_2 \sin\lambda_2 \sin 3\chi_2' \qquad (19b)$$

$$\tau_{p101} = \sigma^{*}_{0,0} \cos\lambda_1 \sin\lambda_1 + A_{\bar{1}01}\, \sigma^{*}_{T,\chi_2'} \cos\lambda_2 \sin\lambda_2 \sin 3\chi_2' \qquad (19c)$$

$$\tau_{p211} = \alpha_2\sigma^{*}_{0,0} \cos\lambda_1 \sin\lambda_1 + A_{\bar{2}11}\, \sigma^{*}_{T,\chi_2'} \cos\lambda_2 \sin\lambda_2 \sin 3\chi_2' \qquad (19d)$$

$$\tau_{p110} = \sigma^{*}_{0,0} \cos\lambda_1 \sin\lambda_1 + A_{\bar{1}01}\, \sigma^{*}_{T,\chi_2'} \cos\lambda_2 \sin\lambda_2 \sin 3\chi_2' \qquad (19e)$$

Substituting into Eq. (1) with the appropriate stress dependence, we have;

$$U_{\bar{1}10} = \frac{A\ Y\ \{1-R\ [\cos\ (60-\chi_1) - A_{\bar{1}01}\sin\ 3\chi_1']\}^{1.85}}{\{1 + R\ A_{\bar{1}01}\ \sin\ 3\chi_1'\}^{1.35}} \qquad (20a)$$

$$U_{\bar{2}11} = \frac{C\ Y\ \{\alpha_2-R[\cos(30-\chi_1') - A_{\bar{2}11}\ \sin\ 3\chi_1']\}^{1.85}}{\{\alpha_2 + R\ A_{\bar{2}11}\ \sin\ 3\chi_1'\}^{1.35}} \qquad (20b)$$

$$U_{\bar{1}01} = \frac{A\ Y\ \{1-R\ [\cos\ \chi_1' - A_{\bar{1}01}\ \sin\ 3\chi_1'\}^{1.85}}{\{1 + R\ A_{\bar{1}01}\ \sin\ 3\chi_1'\}^{1.35}} \qquad (20c)$$

$$U_{\bar{1}\bar{1}2} = \frac{B\,Y\{\alpha_1 - R[\cos(30 + X_1') - A_{\bar{1}\bar{1}2}\sin 3X_1']\}^{1.85}}{\{\alpha_1 + RA_{\bar{1}\bar{1}2}\sin 3X_1'\}^{1.35}} \tag{20d}$$

$$U_{0\bar{1}1} = \frac{A\,Y\{1 - R[\cos(60 + X_1') - A_{\bar{1}01}\sin 3X_1']\}^{1.85}}{\{1 + R\,A_{\bar{1}01}\sin 3X_1'\}^{1.35}} \tag{20e}$$

$$U_{0\bar{1}1} = \frac{A\,Y\{Q - R[\cos 60 - X_2') - A_{\bar{1}01}\sin 3X_2']\}^{1.85}}{\{Q + RA_{\bar{1}01}\sin 3X_2'\}^{1.35}} \tag{21a}$$

$$U_{1\bar{1}2} = \frac{B\,Y\{\alpha_1 Q - R[\cos(30 + X_2') - A_{112}\sin 3X_2']\}^{1.85}}{\{\alpha_1 Q + R\,A_{1\bar{1}2}\sin 3\,{}_2'\}^{1.35}} \tag{21b}$$

$$U_{101} = \frac{A\,Y\{Q - R[\cos X_2' - A_{\bar{1}01}\sin 3X_2']\}^{1.85}}{\{Q + R\,A_{101}\sin 3X_2'\}^{1.35}} \tag{21c}$$

$$U_{211} = \frac{C\,Y\{\alpha_2 Q - R[\cos(30 - X_2') - A_{\bar{2}11}\sin 3X_2']\}^{1.85}}{\{\alpha_2\,Q + R\,A_{\bar{2}11}\sin 3X_2'\}^{1.35}} \tag{21d}$$

$$U_{110} = \frac{A\,Y\{Q - R[\cos(60 - X_2') - A_{101}\sin 3X_2']\}^{1.85}}{\{Q + RA_{\bar{1}01}\sin 3X_2'\}^{1.35}} \tag{21e}$$

where $A = 1.98\times10^{-12}$ ergs $= 2\,U_{k(\bar{1}01)}$ at $\sigma^*_{TC} = 0$

$B = 2.155\times10^{-12}$ ergs $= 2\,U_{k(\bar{1}\bar{1}2)}$ at $\sigma^*_{TC} = 0$

$C = 2U_{k(\bar{2}11)}$ at $\sigma^*_{TC} = 0$, (not determined here experimentally)

$$Y = (\sigma^*_{0,0}\cos\lambda_1\sin\lambda_1)^{\frac{1}{2}}$$

$$R = \sigma^{*}_{T,\chi'}/\sigma^{*}_{0,0}$$

$$Q = \cos\lambda_2 \sin\lambda_2 / \cos\lambda_1 \sin\lambda_1$$

The total strain rate is

$$\dot{\epsilon} = \frac{\rho_1 L_1 b^3 \nu_o}{\pi^2 \Gamma} \cos\lambda_1 \sin\lambda_1 \left(\frac{1}{xx}\right)\Big\{\cos(60-\chi_1')\,\tau^2_{p\bar{1}10}\, e^{-2U_{\bar{1}10}/kT} + \cos(30-\chi_1')\,\tau^2_{p\bar{2}11}\, e^{-2U_{\bar{2}11}/kT} + \cos\chi_1'\,\tau^2_{p\bar{2}01} e^{-2U_{\bar{2}01}/kT} + \cos(30+\chi_1')\,\tau^2_{p\bar{1}\bar{1}2}\, e^{-2U_{\bar{1}\bar{1}2}/kT} + \cos(60+\chi_1')\,\tau^2_{p0\bar{1}1}\, e^{-2U_{0\bar{1}1}/kT}\Big\}$$

$$+ \frac{\rho_{\bar{1}} L_{\bar{1}} b^3 \nu_o}{\pi^2 \Gamma} \cos\lambda_2 \sin\lambda_2 \left(\frac{1}{zz}\right)\Big\{\cos(60+\chi_2')\,\tau^2_{p0\bar{1}1}\, e^{-2U_{0\bar{1}1}/kT} + \cos(30+\chi_2')\,\tau^2_{p1\bar{1}2}\, e^{-2U_{1\bar{1}2}/kT} + \cos\chi_2'\,\tau^2_{p101}\, e^{-2U_{101}/kT} + \cos(30-\chi_2')\,\tau^2_{p211}\, e^{-2U_{211}/kT} + \cos(60-\chi_2')\,\tau^2_{p110}\, e^{-2U_{110}/kT}\Big\} \qquad (22)$$

where $xx = \Big(\tau_{p\bar{1}10}\, e^{-U_{\bar{1}10}/kT} + \tau_{p\bar{2}11}\, e^{-U_{\bar{2}11}/kT} + \tau_{p\bar{1}01}\, e^{-U_{\bar{1}01}/kT} + \tau_{p\bar{1}\bar{1}2}\, e^{-U_{\bar{1}\bar{1}2}/kT} + \tau_{p0\bar{1}1}\, e^{-U_{0\bar{1}1}/kT}\Big)$

$$zz = \Big(\tau_{p0\bar{1}1}\, e^{-U_{0\bar{1}1}/kT} + \tau_{p1\bar{1}2}\, e^{-U_{1\bar{1}2}/kT} + \tau_{p101}\, e^{-U_{101}/kT} + \tau_{p211}\, e^{-U_{211}/kT} + \tau_{p110}\, e^{-U_{110}/kT}\Big)$$

If all the pre-exponential terms and the parameters A's and α's are known, we can solve Eq. (22) by the trial and error method for a given set of temperature strain rate condition.

The values of the asymmetric factor A and α can be estimated by the following method (Fig. 15). First extrapolate the normal yield stresses to 0°K as is done in Fig. 6. Resolve these normal stresses to the slip planes observed experimentally at 77°K. The slip planes usually converge to a single crystallographic slip plane from high temperature to 77°K as shown in Figs. 8-13. Therefore, we can assume that at 0°K these are the operative slip planes also. Furthermore, since there is no thermal activation at 0°K, slip always taks place on the plane which is the easiest for slip to occur. Therefore, the extrapolated values of normal stress resolved on observed slip planes are the critical resolve shear stress at 0°K, i.e. τ_p's. Plot these resolved shear stress versus the function $\sigma^*_{0,}\ \chi' \cos\lambda \sin\lambda$, as shown in Eqs. (18) and (19), and Fig. 15. The slope of this plot should give the asymmetric factor A, the intersects with the ordinate should give the α values. This method works only if the asymmetric factors have linear dependence on the stress as is assumed in the model. Shown in Fig. 15, there are four points that slip on {101} planes, and they almost all fall on one straight line giving the asymmetric factor $A_{\bar{1}01}$ value of 0.263. The asymmetry on {112} planes is smaller, and the slope gives $A_{\bar{1}\bar{1}2} = .125$ and $\alpha_1 = .894$ from the intersect. Also noted from Fig. 15 is the assumption that linear stress dependence of A is a reasonable one. The "X" marks depict the stressed resolved on other possible slip planes that slip did not actually occur; they all fall below the straight lines as expected since the straight lines represent

the critical resolved shear stresses for slip. From slip traces analysis, we note that $(\bar{2}11)$ plane is never operative. This suggests that $(\bar{2}11)$ plane has an exceptionally high Peierls stress ($\tau_{p\bar{2}11}$) that slip always takes place on some other planes where the Peierls stresses are lower. This observation agrees with the calculation of Hirth and Lothe.[25] With this information, we can analyze the result with the aid of a computer.

Since $(\bar{2}11)$ and (211) are not observed at small strains, they can be ignored in Eq. (22). This reduces to only eight the terms to be considered. The pre-exponential terms can be estimated as follows: (1) Calculate the yield stress-temperature relationship for only one operative slip system indicated by the experimental slip trace analysis at low temperatures for a given orientation. This is a straight forward calculation making use of the relation $U_n/2U_k \simeq T/T_c$ [12] and assuming constant pre-exponential term. (2) Select the highest temperature where the experimental slip trace analysis still indicates only one crystallographic slip plane. (3) Calculate the pre-exponential term using Eq. (22) for single slip substituting in the selected temperature and the stress obtained from step 1 for that temperature. We will use this value of pre-exponential term for all temperatures. Since the pre-exponential terms are known, we can proceed to solve the strain rate equation as follows: (1) Select a temperature [usually start from 450°K(Tc)], assume a stress value and substitute this into probable slip terms $e^{-2U_{hk\ell}/kT}$. (2) Calculate the value of the right hand side of Eq. (22). (3) Compare this value with the total strain rate, if it is not within 0.02×10^{-5} of $\dot{\epsilon}$ total, assume a new stress value and repeat the calculation. (4) If this value is within

the tolerance, calculate ψ_1 and ψ_2. Select a lower temperature and repeat from step 1.

At high temperatures, quite a few slip terms $e^{-2U_{hk\ell}/kT}$ have to be considered, since their magnitudes are comparable. As the temperature decreases, a single slip term begins to prevail. At the temperature where the experimental slip traces start to indicate single slip the other slip terms are usually less than 1/100 of the prevailing slip term for single slip and can be neglected. At even lower temperature, the values of other slip terms drop off sharply. The calculated results of the yield stress-temperature relationship and the slip geometry are shown in Figs. 16 and 17.

V. DISCUSSION OF RESULTS

The agreement between predicted and experimental results of the yield stress-temperature relationship for all six orientations is best for $X_1'=0$ ("B"). For this orientation, only the $(\bar{1}01)$ [111] slip system is activated below room temperature. For higher temperatures a slight amount of $(\bar{1}\bar{1}2)$[111] system also contributes to the macroscopic plastic strain. Since the X' value is zero the model predicts no perturbation of the Peierls hill, and the true Peierls mechanism should work for the temperature range below 300°K. This good agreement is expected as indicated by a previous work.[26] For orientations other than $X_1'=0$, small deviations were obtained between the experimentally determined and predicted values. The poorest agreement arises from orientation C ($X_1'=+28°$), where the experimental curve crosses the curves for $X_1'=+16°$ and $X_1'=0°$. The discrepancy might be attributed to an anomalous Peierls hill shape and by a different perturbation by the applied stress, than that assumed in the model. The agreement for orientation "G" ($X_1'=-4°$ $X_2'=-5°$) is also not as good as the others. For this orientation, at least four slip systems $\left((\bar{1}01)[111], (\bar{1}\bar{1}2)[\bar{1}11], (101)[\bar{1}11], (1\bar{1}2)[\bar{1}11]\right)$ were activated at most of the temperatures and complexity of the slip systems may have caused same differences.

The predictions of slip geometry agree well with the experimental facts. For orientations "A", "B", "C", and "D" only one slip direction is observed, for orientations "E" ($X_2'=-13°$) and "G" ($X_1'=-4°$), two slip directions are observed ([111],[$\bar{1}$11]) as indicated in Fig. 17. For orientation "E", the model predicts equal contribution from both slip directions from 450°K to 280°K, more [111]slip from 280°K to 150°K and

only [111] slip from 180°K to 0°K. For orientation "G", equal contribution from both slip directions from 450°K to 165°K, more [111] slip from 165°K to 100°K, much more [111] slip from 100°K to 40°K, and only [111] slip from 40°K to 0°K. These predictions agree well with observed facts.

Considering the agreement between the observed and predicted results, the modified Peierls model seems to provide a relatively successful approach to the subject of low temperature deformation of Mo single crystals. The merits of this model lie in the very simple assumptions made on the perturbation of Peierls stress by the applied stress. In spite of the very complex nature of dislocation core, e.g. the splitting geometry before and after the stress is applied, the change of Peierls stress due to the applied stress and the twinning antitwinning consideration, the simple linear approach of this model has been quite successful. The parameters of this model (e.g. A and α, etc.) can be easily deduced from experiments, having the advantage over the cross slip model where stacking fault energies are unknown. A complete model accounting for every detail of the plastic behavior will have to wait unit much more knowledge of the dislocation core is gained.

VI. SUMMARY

(1) The plastic behavior of Mo single crystals for six orientations has been investigated over the range from ~20°K to 550°K. The yield strength and slip geometry are found to be very assymetric.

(2) A modified Peierls model is used for the rationalization of the experimental results. The model is based on the concept of core splitting of screw dislocations.

(3) The theoretical predictions of yield strength and slip geometry are reasonably accurate.

(4) While the nominal validity of this model is established, much has to be learned on the dislocation core before a more sophisticated model can be formulated.

ACKNOWLEDGEMENTS

The author is very grateful to Professor John E. Dorn for his guidance and encouragement during his graduate studies and this investigation, to Professor G. Thomas for his introduction of Materials Science to the author, and continuous interests and guidance.

Thanks are also due to Professor C. Tobias for manuscript review, Professor A. K. Mukherjee and Mr. G. Liu for helpful discussions, Mrs. G. Pelatowski for line drawings and to Miss Jane Ball for typing this report.

This work was done under the auspices of the United States Atomic Energy Commission through the Inorganic Materials Research Division of the Lawrence Radiation Laboratory.

REFERENCES

1. F. Kroupa and V. Vitek, Can. J. Phys., 1967, Vol. 45, No. 2, Part 3, p. 945.
2. B. Escaig, G. Fontain and J. Friedel, Can. J. Phys. 1967, Vol. 45, No. 2, Part 2, 481.
3. M. S. Duesbery and P. B. Hirsch: Dislocation Dynamics (McGraw Hill N. Y. 1968) p. 57.
4. T. Taoka, S. Takeuchi and E. Furubayashi, J. Phys. Soc. Japan, 1964, Vol. 19, p. 701.
5. D. F. Stein, Can. J. Phys. 1967, Vol. 45, No. 2, Part 3, p. 1063.
6. P. J. Sherwood, F. Guiu, H. C. Kim and P. L. Pratt, Can. J. Phys., 1967, Vol 45, No. 2, part 3, p. 1075.
7. B. Sestak and N. Zarubova, Phys. Stat. Sol., 1965, Vol. 10, p. 239.
8. B. Sestak, N. Zarubova and V. Sladek, Can. J. Phys., 1967, Vol. 45, No. 2, Part 3, p. 1031.
9. D. R. Bowen, J. W. Christian, and G. Taylor, Can. J. Phys., 1967, Vol. 45, No. 2, Part 3, p. 903.
10. A. S. Keh and Y. Nakada, Can. J. Phys. 1967, Vol. 45, No. 2, Part 3, p. 1101.
11. R. A. Foxall, M. S. Duesbery, and P. B. Hirsch, Can. J. Phys. 1967, Vol. 45, No. 2 Part 2, p. 607.
12. P. Guyot and J. E. Dorn, Can. J. Phys. 1967, Vol. 45, No. 2, Part 3 p. 983.
13. A. S. Keh, Phil Mag. 1965, Vol. 12, p.9.
14. A. Lawley and H. L. Graigher, Phil. Mag. 1964, Vol. 10, p. 15.
15. G. Taylor and J. W. Christian, Phil. Mag. 1967, Vol. 15, p. 873.
16. J. E. Dorn and A. K. Mukherjee, Trans. AIME (to be published).

17. D. Vesely, Phys. Stat. Sol., 1968, Vol. 29, p. 675.

18. D. Vesely, Phys. Stat. Sol., 1968, Vol. 29 p. 685.

19. G. Liu, Dept. of Mat. Sci. and Eng., Univ. of Calif. Berkeley. Private communication.

20. L. Kaun, A. Luft, J. Richter and D. Schulze, Phys. Stat. Sol. 1968, Vol. 26, No. 2, p. 485.

21. S. S. Lau and J. E. Dorn, Scripta Met. 1968, Vol. 2, p. 335.

22. Y. Nakada and A. S. Keh: Acta Met., 1968, Vol. 16, p. 903.

23. V. Vitek, Phil. Mag. 1968, Vol. 18, No. 154, p. 773.

24. J. E. Dorn and S. Rajnak, Trans. AIME, Vol. 230, p. 1052

25. J. P. Hirth and J. Lothe, Phys. Stat. Sol. 1966, Vol. 15, p. 487.

26. S. S. Lau, S. Ranji, A. K. Mukherjee, G. Thomas, and J. E. Dorn, Acta Met., 1967, Vol. 15, p. 237.

27. B. L. Mordike and P. Haasen, Phil. Mag. 1962, Vol. 7, p. 459.

28. R. L. Heischer, J. Appl. Phys., 1962, Vol. 33, No. 12, p. 3504.

29. Y. Nakada and A. S. Keh, Acta. Met., 1968, Vol. 16, p. 903.

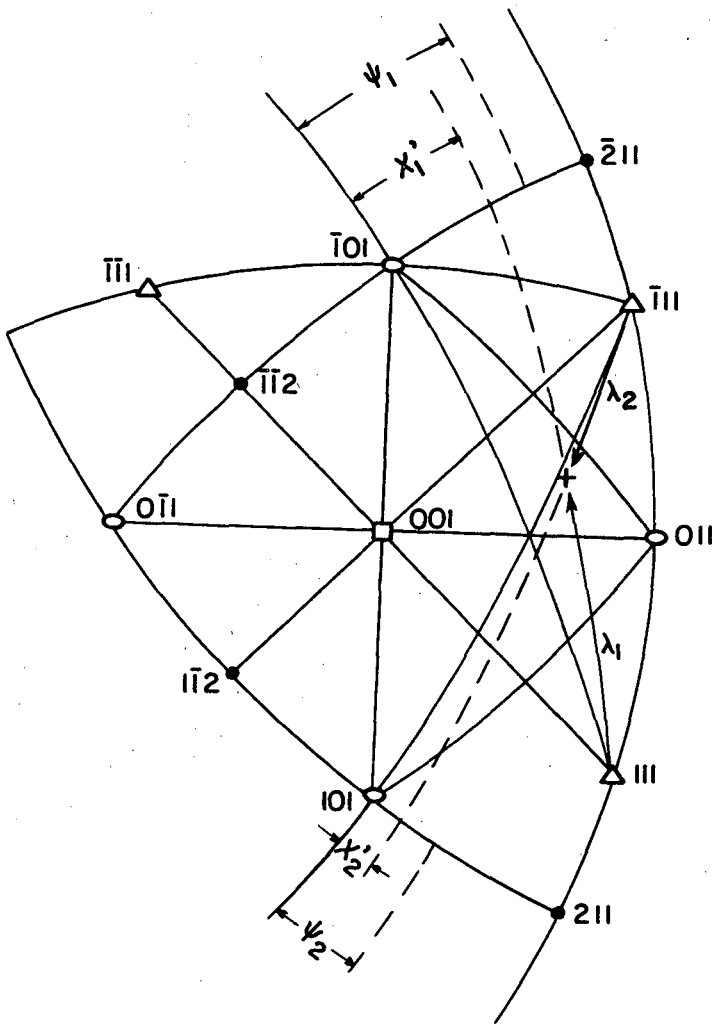

FIG. 1 STANDARD STEREOGRAPHIC PROJECTION. (+ IS THE POLE OF THE SPECIMEN AXIS; ψ_1 AND χ_1' ARE THE ANGLES THAT THE OBSERVE PLANE OF SLIP AND THE PLANE OF MAXIMUM SHEAR STRESS MAKE WITH $(\bar{1}01)$ PLANE, RESPECTIVELY. THE SCHMID ANGLE FOR SLIP IN THE [111] DIRECTION IS λ_1. SIMILARLY FOR χ_2, ψ_2' AND λ_2 WITH RESPECT TO (101) PLANE AND [111] DIRECTION.)

XBL 694-391

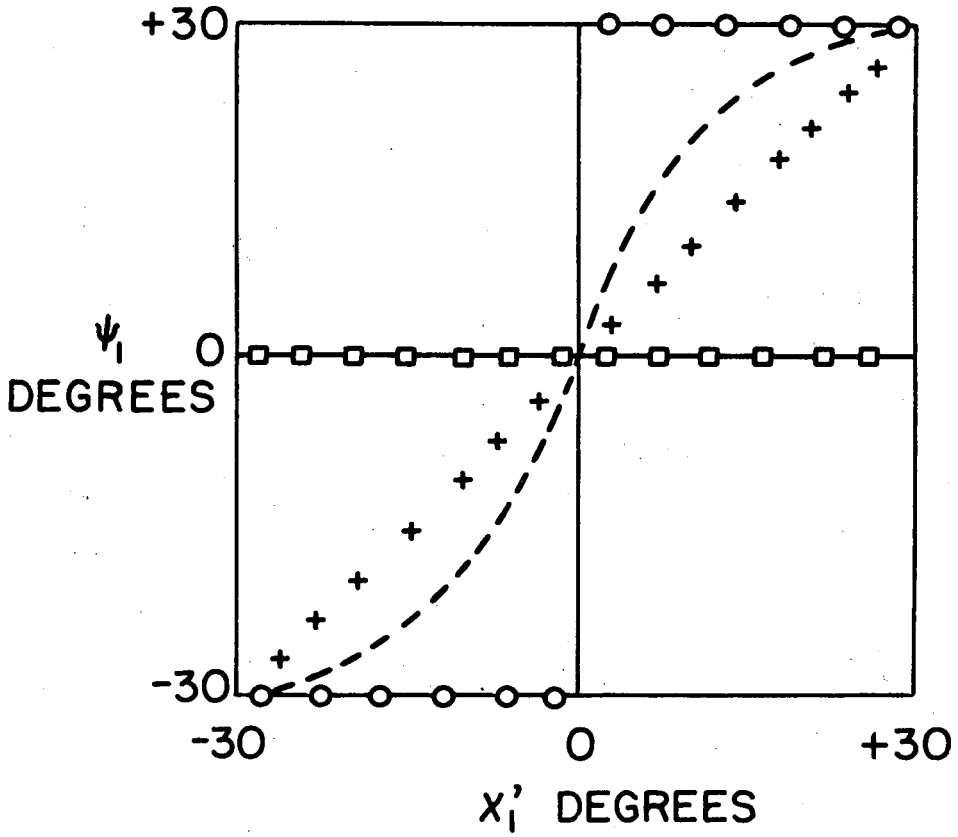

FIG. 2 SYMMETRIC SLIP.

XBL 694-392

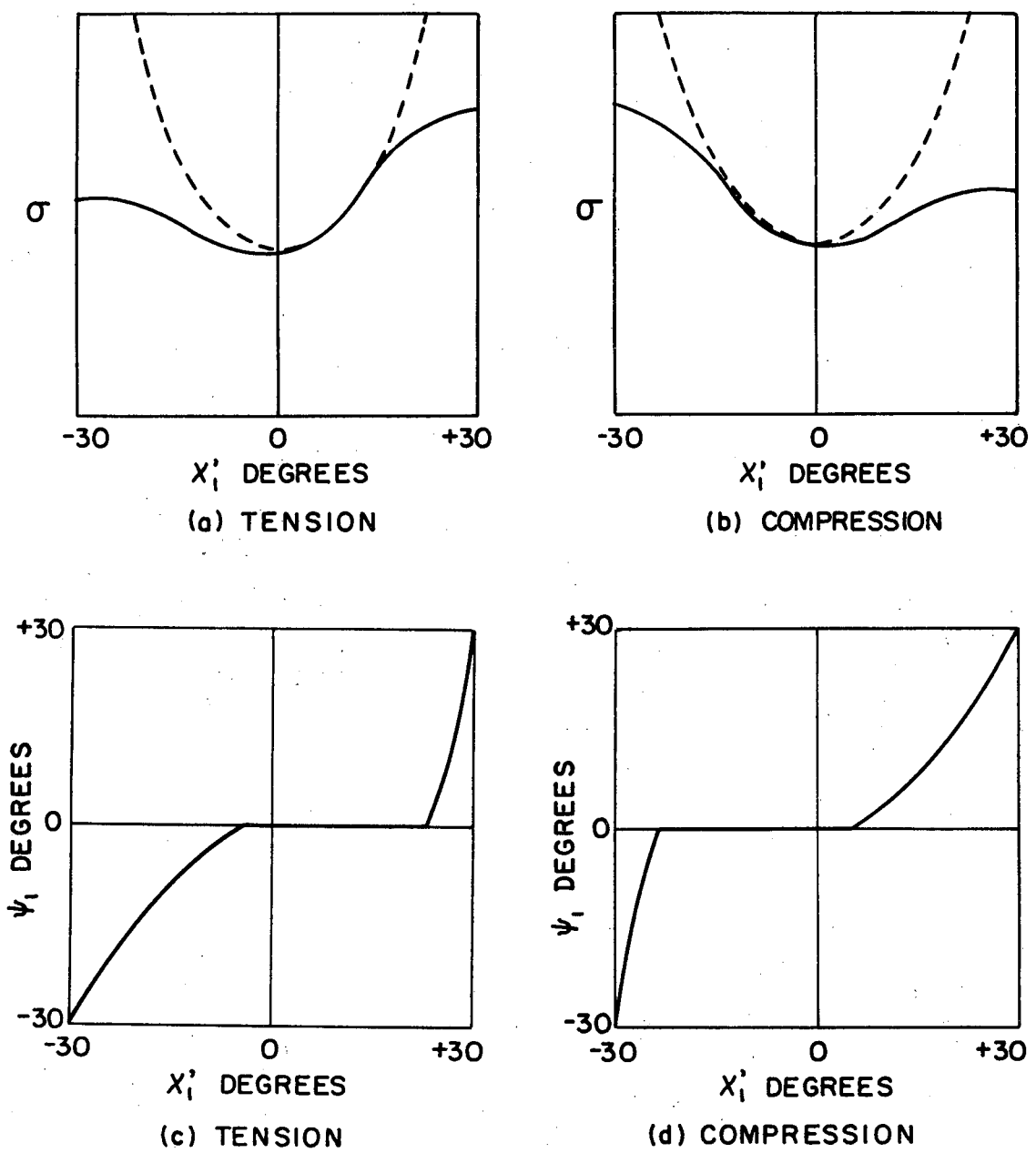

FIG. 3 SCHEMATIC REPRESENTATION OF ASYMMETRIC BEHAVIOR.

XBL 694-396

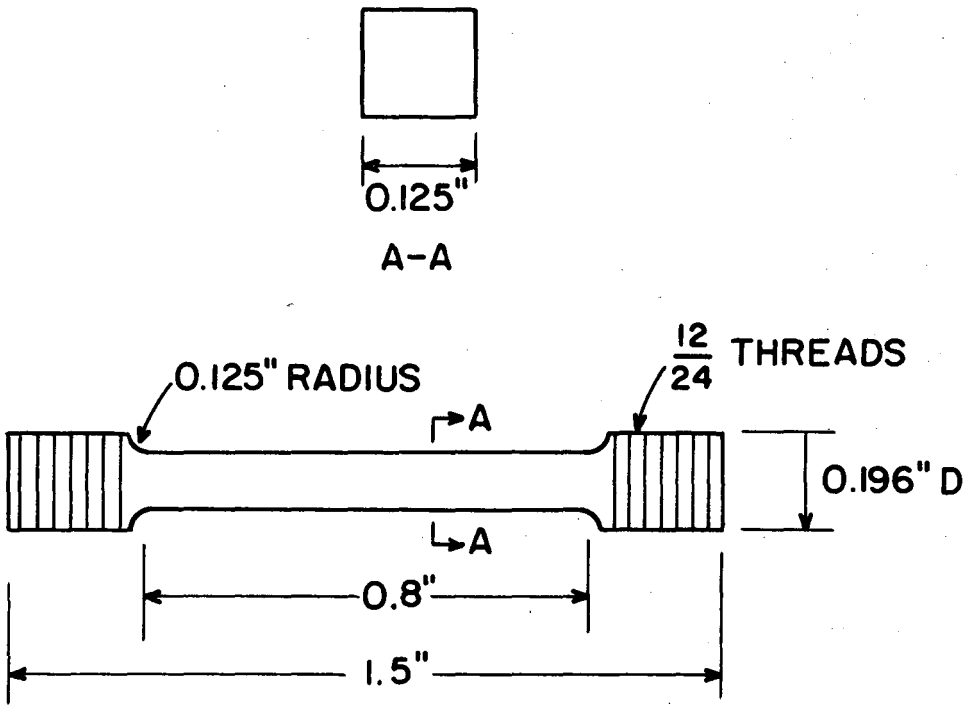

FIG. 4 DIMENSIONS OF THE SPECIMEN.

XBL 694-393

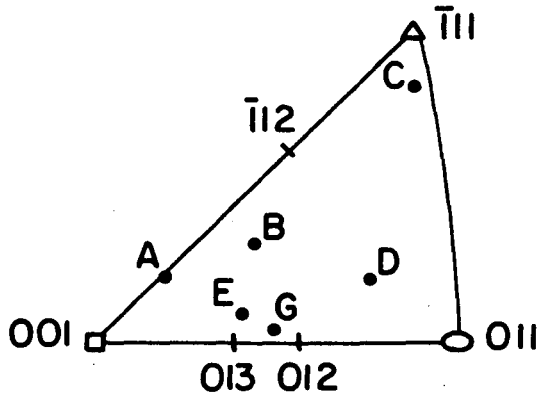

FIG. 5 ORIENTATIONS OF THE SPECIMENS.

XBL 694-394

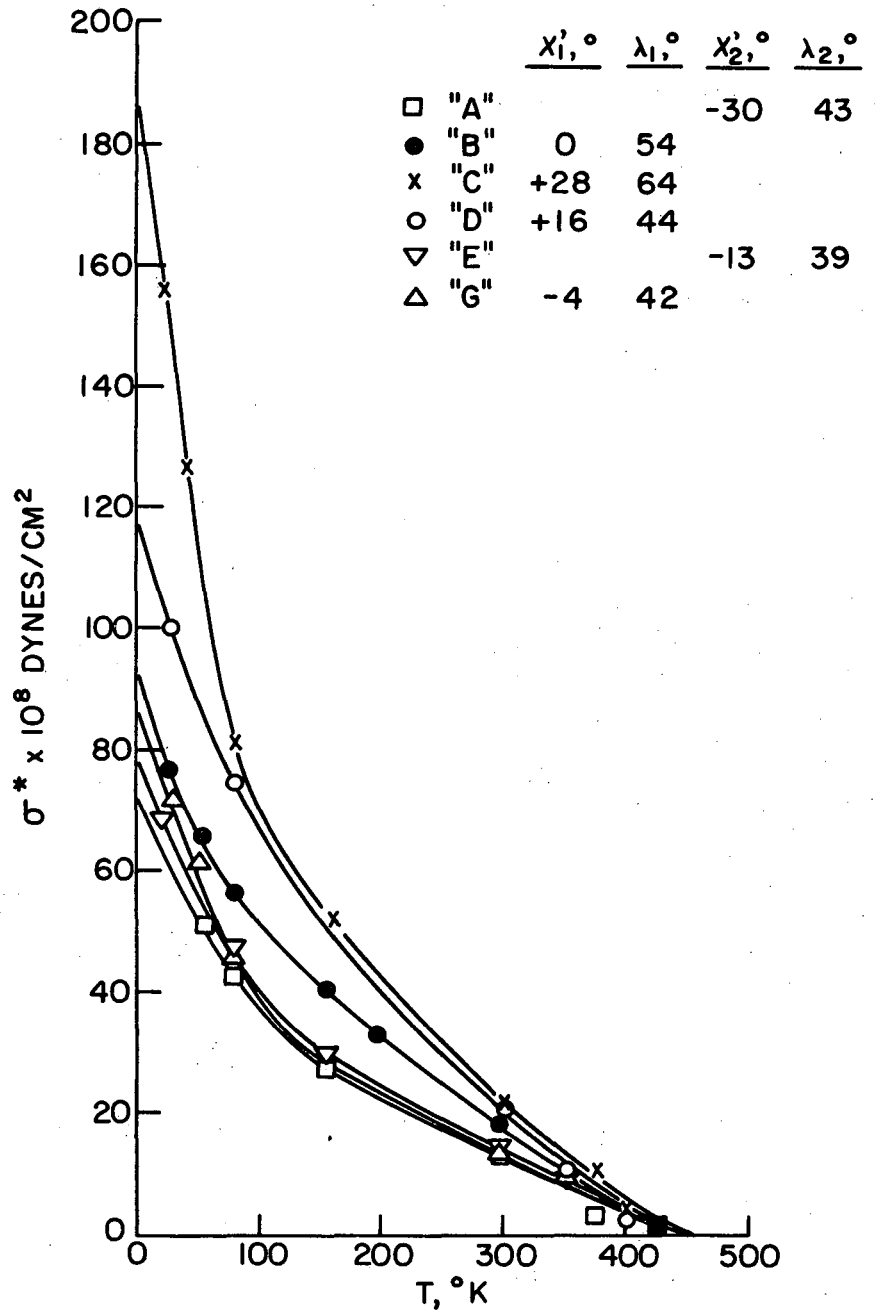

FIG. 6 THE THERMALLY ACTIVATED COMPONENT OF NORMAL STRESS vs. TEMPERATURE.

XBL 694-395

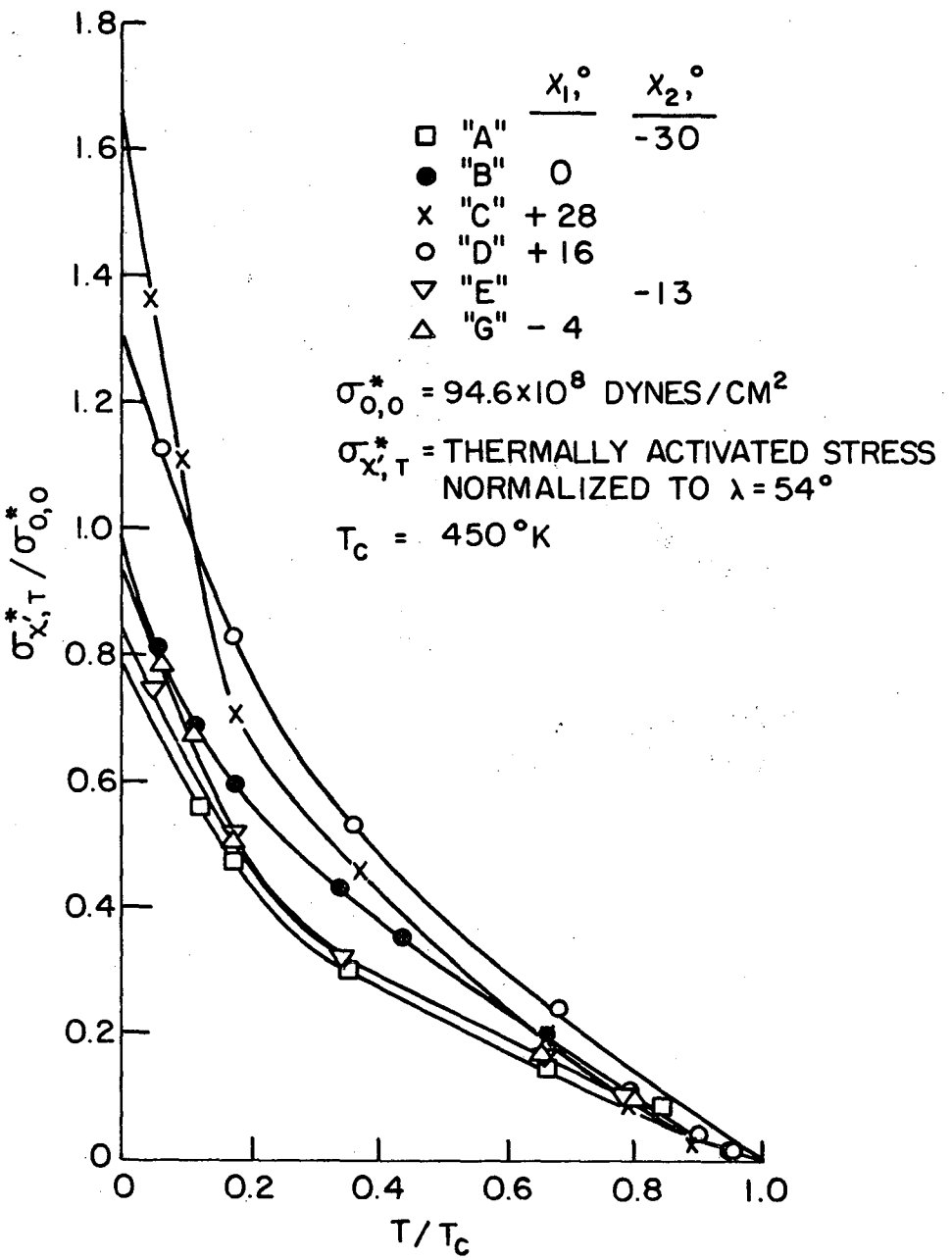

FIG. 7 REDUCED STRESS (SCHMID ANGLE λ NORMALIZED TO 54°) vs. REDUCED TEMPERATURE.

XBL 694-397

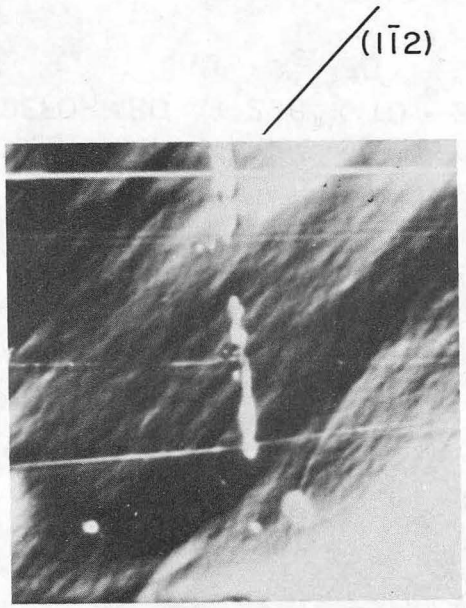

FIG. 8a SLIP TRACES OF SPECIMEN (A3L) DEFORMED AT 77°K TO 5.3% ELONGATION. $X_2' = -30°$ "A"

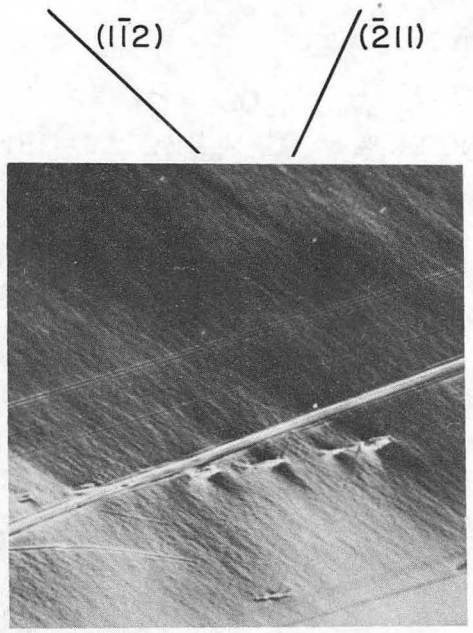

FIG. 8b SLIP TRACES OF SPECIMEN (A4S) DEFORMED AT 158°K TO 13.6% ELONGATION. $X_2' = -30°$ "A"

XBB 694-2466

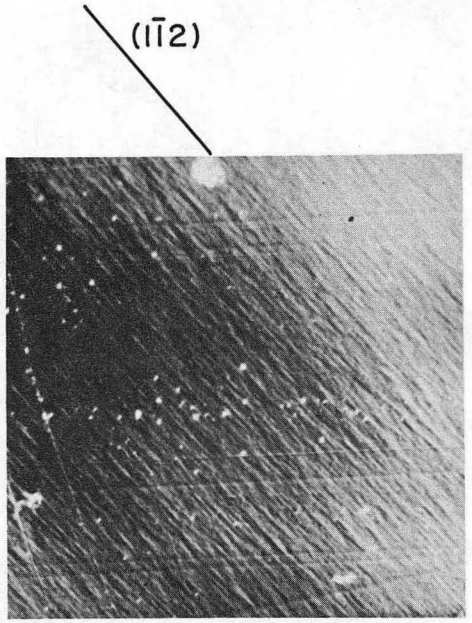

FIG. 8c SLIP TRACES OF SPECIMEN (A1L) DEFORMED AT 298°K TO 5.5% ELONGATION. $X_2' = -30°$ "A"

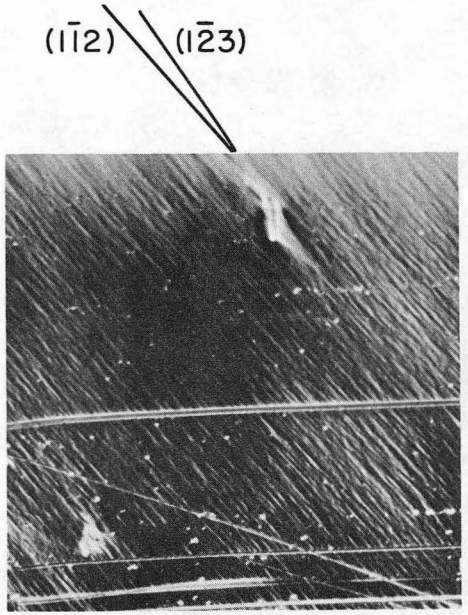

FIG. 8d SLIP TRACES OF SPECIMEN (A8L) DEFORMED AT 375°K TO 4% ELONGATION. $X_2' = -30°$ "A"

XBB 694-2467

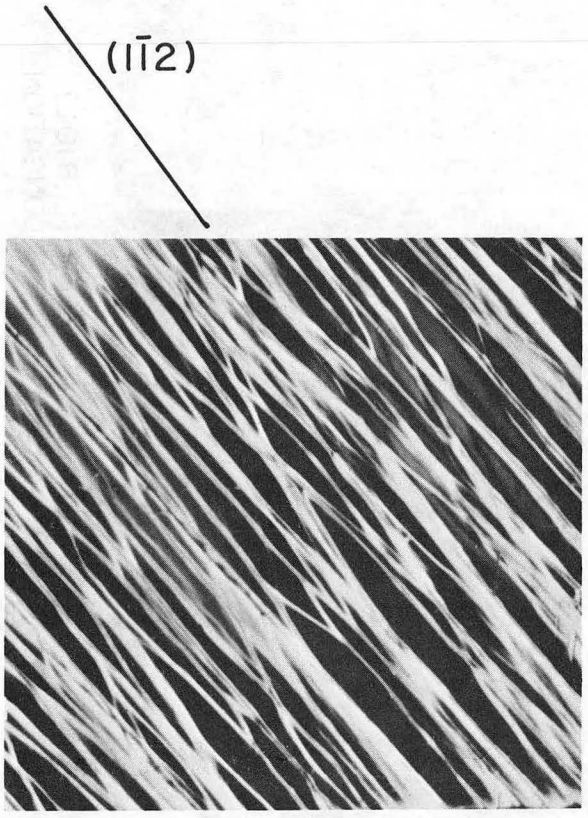

FIG. 8e SLIP TRACES OF SPECIMEN (A2S) DEFORMED AT 550°K TO 5% ELONGATION.
$X_2' = -30°$ "A"

XBB 694-2465

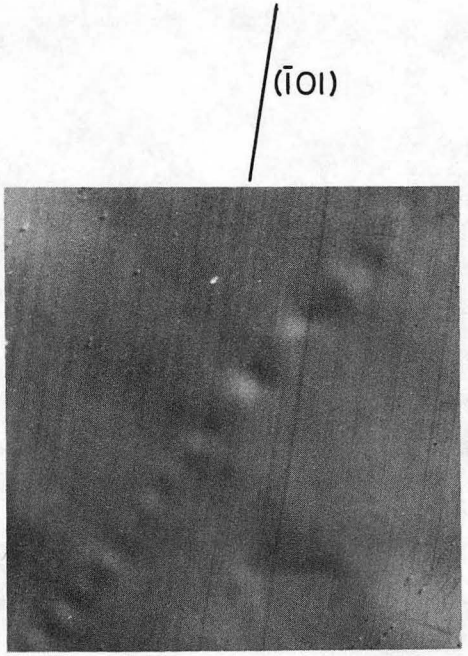

FIG. 9a SLIP TRACES OF SPECIMEN (B11S) DEFORMED AT 77°K TO 0.05% ELONGATION.
$X_1' = 0$ "B"

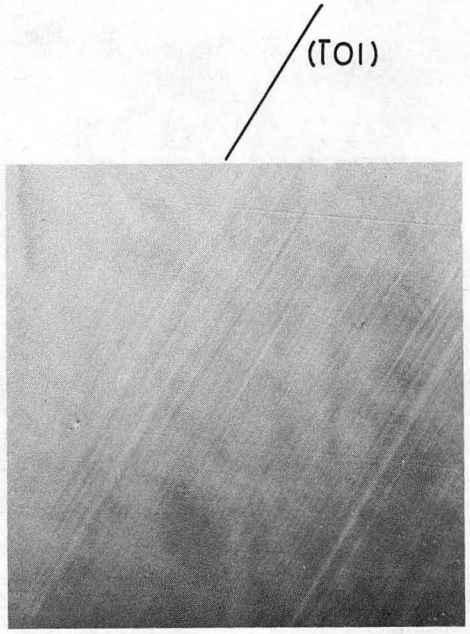

FIG. 9b SLIP TRACES OF SPECIMEN (B10L) DEFORMED AT 298°K TO 0.04% ELONGATION.
$X_1' = 0$ "B"

XBB 694-2468

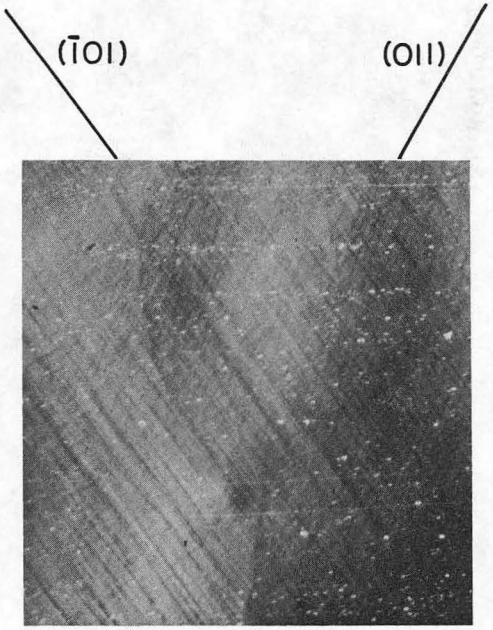

FIG. 9c SLIP TRACES OF SPECIMEN (B7S) DEFORMED AT 325°K TO 2.5% ELONGATION.
$X_1' = 0$ "B"

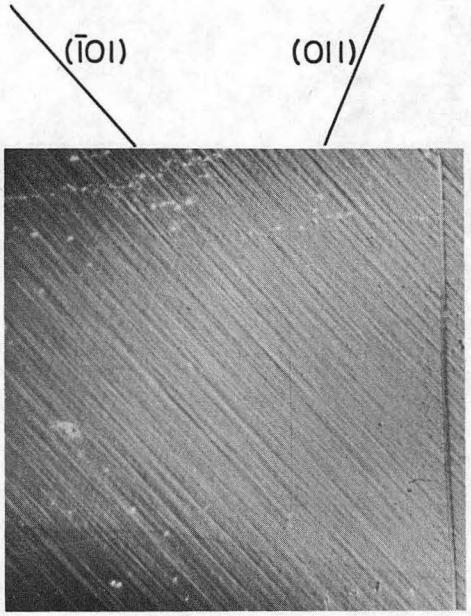

FIG. 9d SLIP TRACES OF SPECIMEN (B4OPP.L) DEFORMED AT 356°K TO 6% ELONGATION.
$X_1' = 0$ "B"

XBB 694-2469

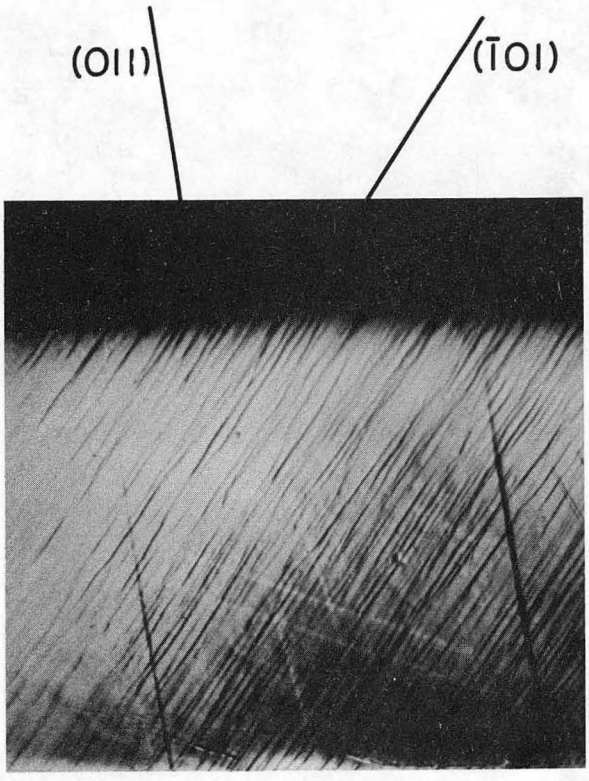

FIG. 9e SLIP TRACES OF SPECIMEN (B 2L) DEFORMED AT 550°K TO 3% ELONGATION.
$X_1' = 0$ "B"

XBB 694-2464

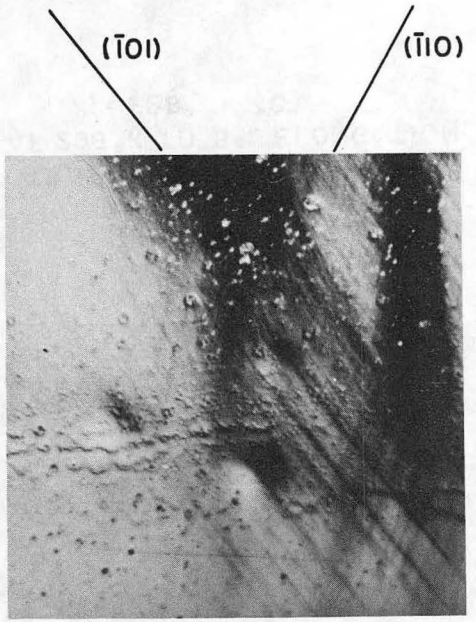

FIG. 10a SLIP TRACES OF SPECIMEN (GLA2S) DEFORMED AT 77°K TO 1% ELONGATION.
$X_1' = +28°$ "C"

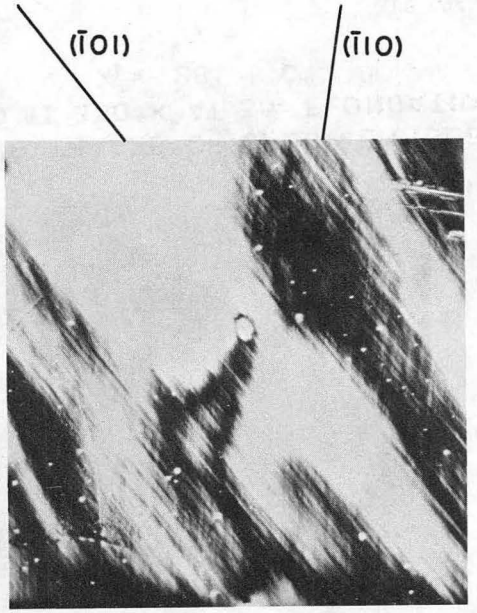

FIG. 10b SLIP TRACES OF SPECIMEN (GLC18S) DEFORMED AT 160°K TO 2.5% ELONGATION.
$X_1' = +28°$ "C"

XBB 694-2470

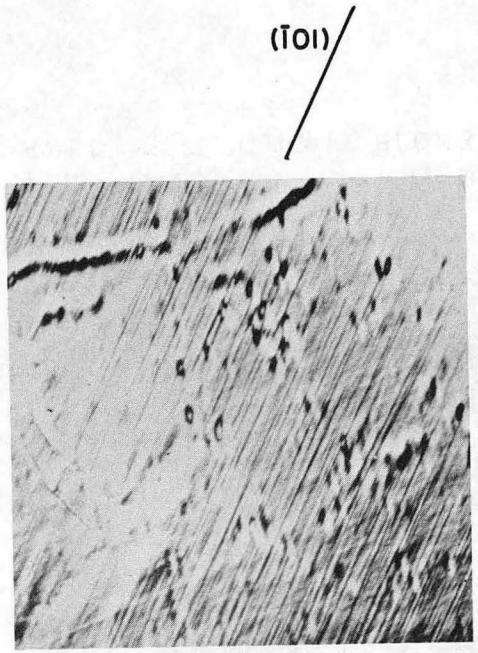

FIG. 10c SLIP TRACES OF SPECIMEN (GL AIL) DEFORMED AT 298°K TO 5% ELONGATION.
$X_1' = +28°$ "C"

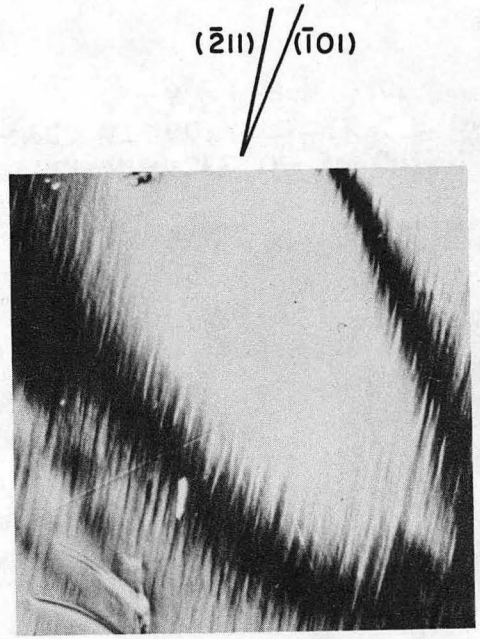

FIG. 10d SLIP TRACES OF SPECIMEN (GL B9S) DEFORMED AT 350°K AT 3% ELONGATION)
$X_1' = +28°$ "C"

XBB 694-2471

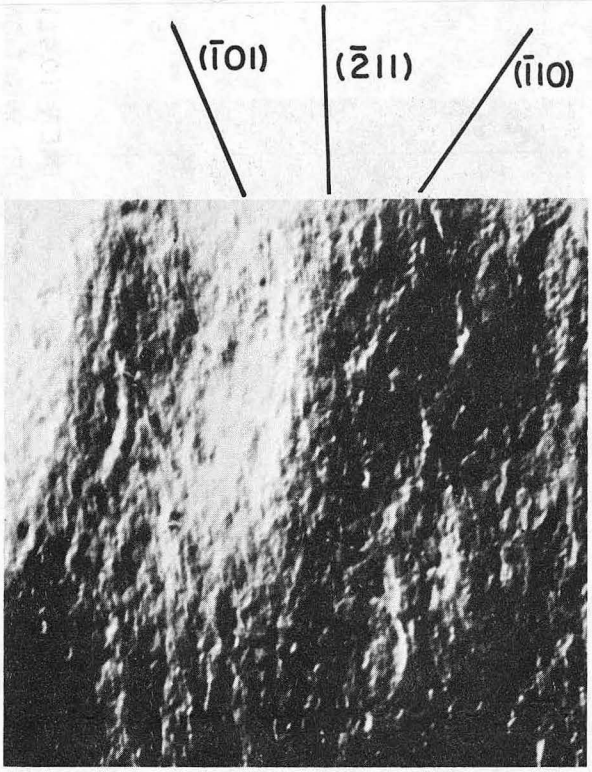

FIG. 10e SLIP TRACES OF SPECIMEN (GLASS) DEFORMED AT 453°K TO 3% ELONGATION.
$X_1' = +28°$ "C"

XBB 694-2462

FIG. 11a SLIP TRACES OF SPECIMEN (D2S) DEFORMED AT 77°K TO 0.46% ELONGATION. $X_1' = +16°$ "D"

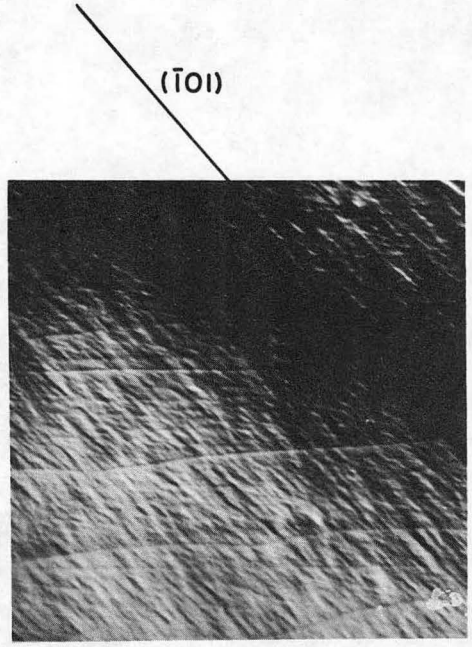

FIG. 11b SLIP TRACES OF SPECIMEN (D4L) DEFORMED AT 298°K TO 2.7% ELONGATION. $X_1' = +16°$ "D"

XBB 694-2473

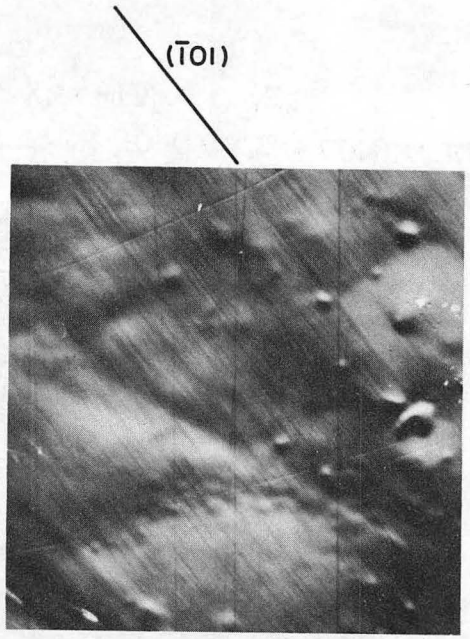

FIG. 11c SLIP TRACES OF SPECIMEN (D3S) DEFORMED AT 351°K TO 0.53% ELONGATION.
$X_1' = +16°$ "D"

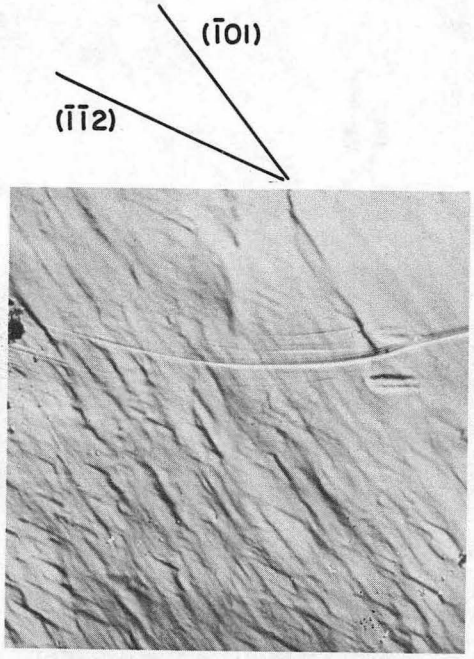

FIG. 11d SLIP TRACES OF SPECIMEN (D1L) DEFORMED AT 550°K TO 0.405% ELONGATION.
$X_1' = +16°$ "D"

XBB 694-2474

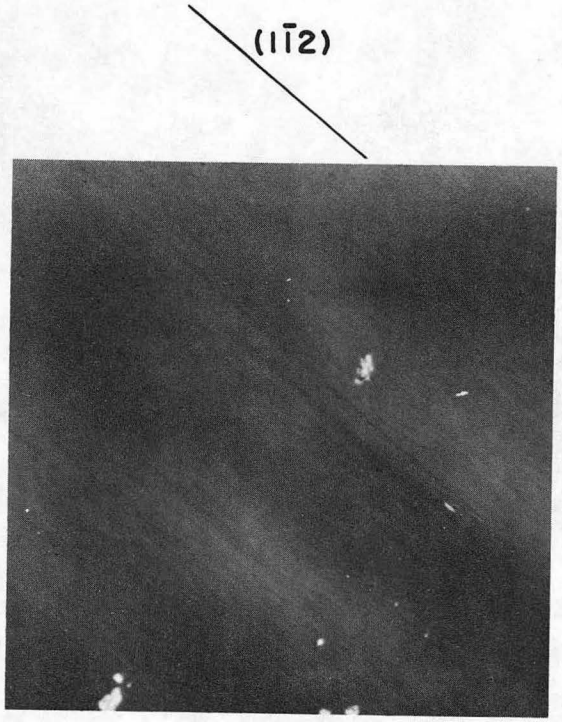

FIG. 12a SLIP TRACES OF SPECIMEN (E8S) DEFORMED AT 77°K TO 0.05% ELONGATION.

$X_2' = -13°$ "E"

FIG. 12b SLIP TRACES OF SPECIMEN (E5L) DEFORMED AT 153°K TO 0.3% ELONGATION.

$X_2' = -13°$ "E"

XBB 694-2475

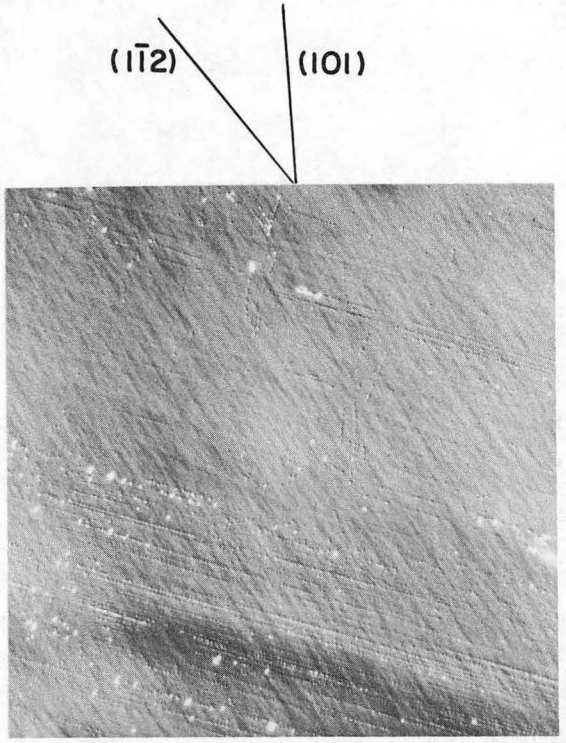

FIG. 12c SLIP TRACES OF SPECIMEN (E9L) DEFORMED AT 298°K TO 1% ELONGATION.
X_2' = -13° "E"

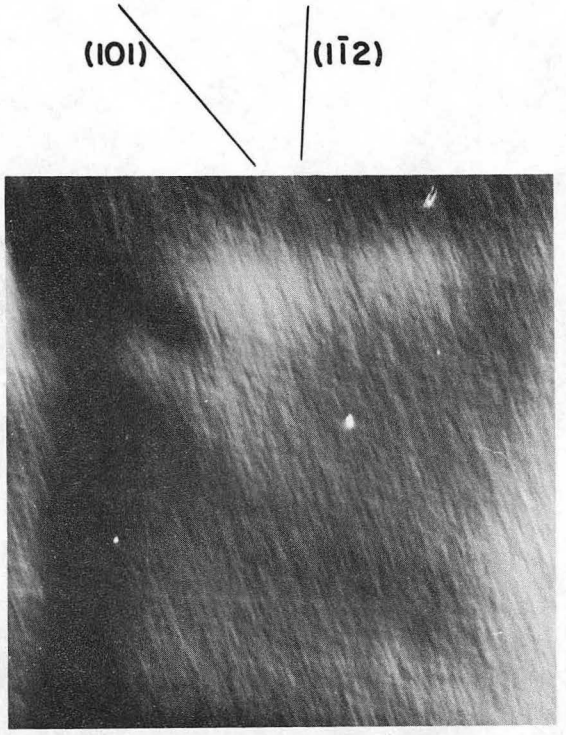

FIG. 12d SLIP TRACES OF SPECIMEN (E7L) DEFORMED AT 352°K TO 0.2% ELONGATION.
X_2' = -13° "E"

XBB 694-2472

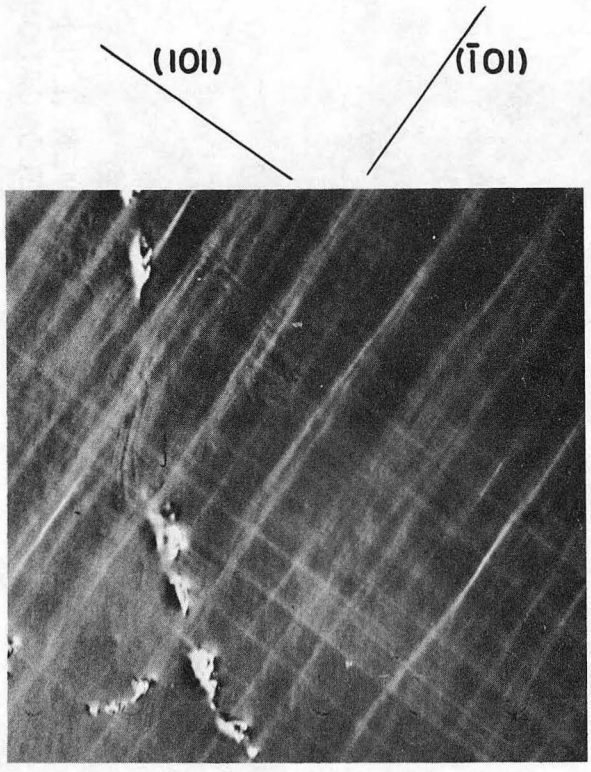

FIG. 12e SLIP TRACES OF SPECIMEN (E1S) DEFORMED AT 550°K TO 0.5% ELONGATION.

$X_2' = -13°$ "E"

XBB 694-2463

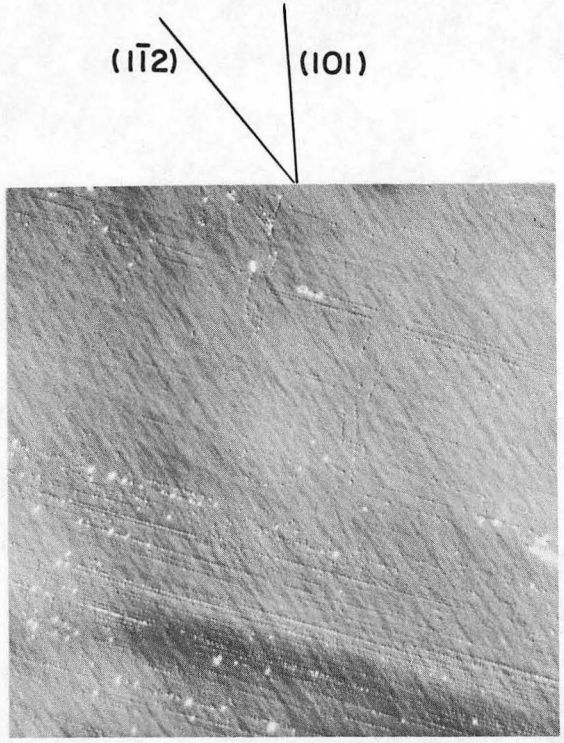

FIG. 12c SLIP TRACES OF SPECIMEN (E9L) DEFORMED AT 298°K TO 1% ELONGATION.
X_2' = -13° "E"

FIG. 12d SLIP TRACES OF SPECIMEN (E7L) DEFORMED AT 352°K TO 0.2% ELONGATION.
X_2' = -13° "E"

XBB 694-2472

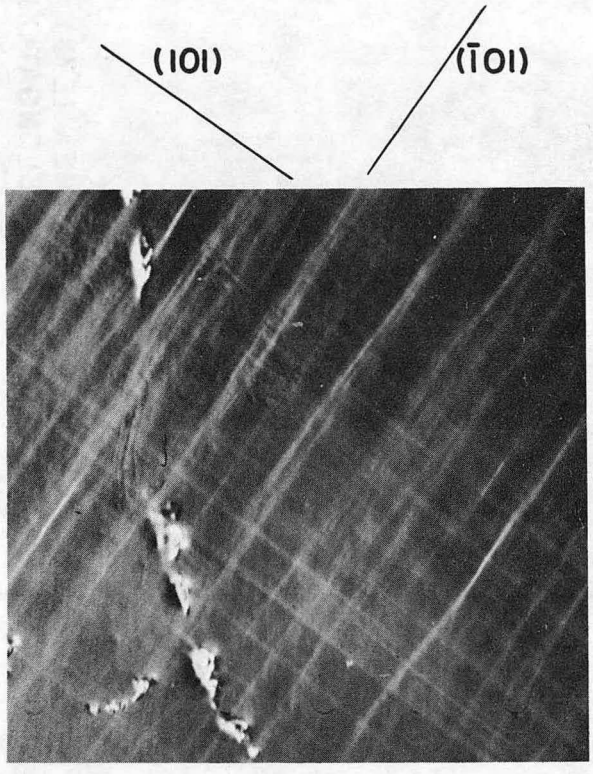

FIG. 12e SLIP TRACES OF SPECIMEN (E1S) DEFORMED AT 550°K TO 0.5% ELONGATION.

$X_2' = -13°$ "E"

XBB 694-2463

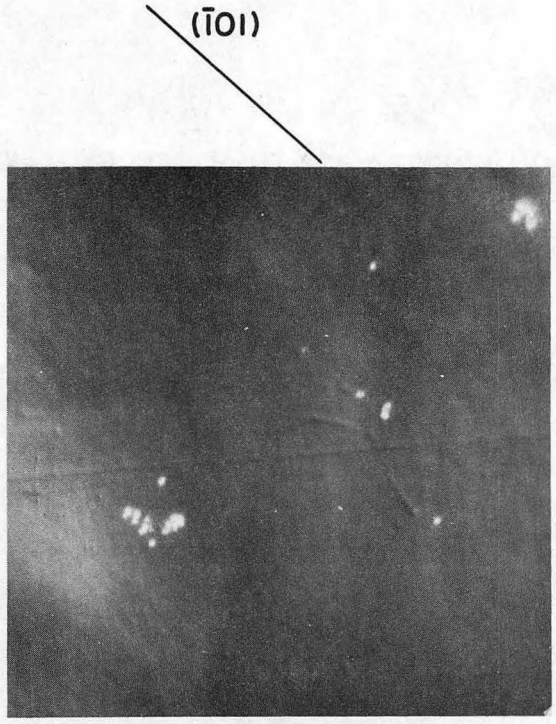

FIG. 13a SLIP TRACES OF SPECIMEN G6L DEFORMED AT 77°K TO 1.1% ELONGATION.

$\chi_1' = -4°$ "G"

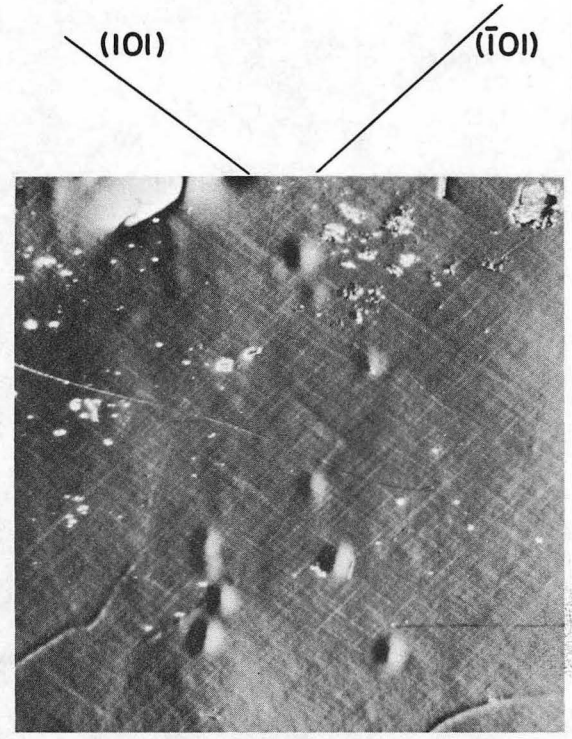

FIG. 13b SLIP TRACES OF SPECIMEN G4L DEFORMED AT 298°K TO 2.5% ELONGATION.

$\chi_1' = -4°$ "G"

XBB 694-2476

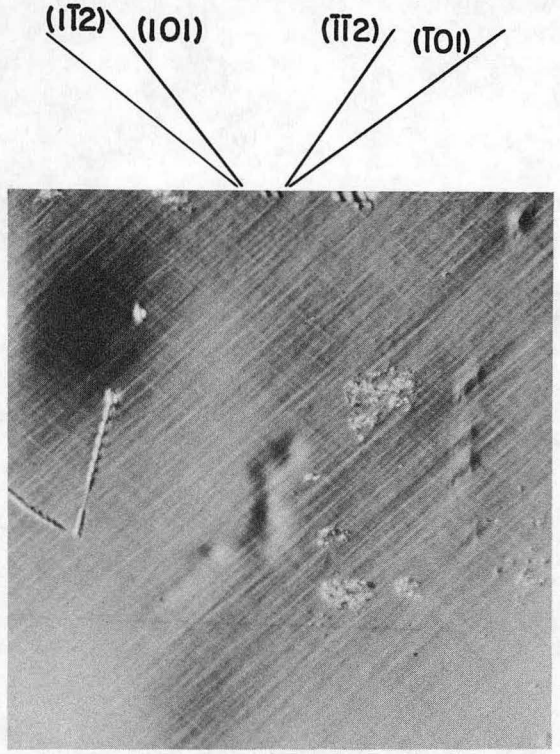

FIG. 13c SLIP TRACES OF SPECIMEN G 7L
DEFORMED AT 350°K TO 2.5% ELONGATION.

$X_1' = -4°$ "G"

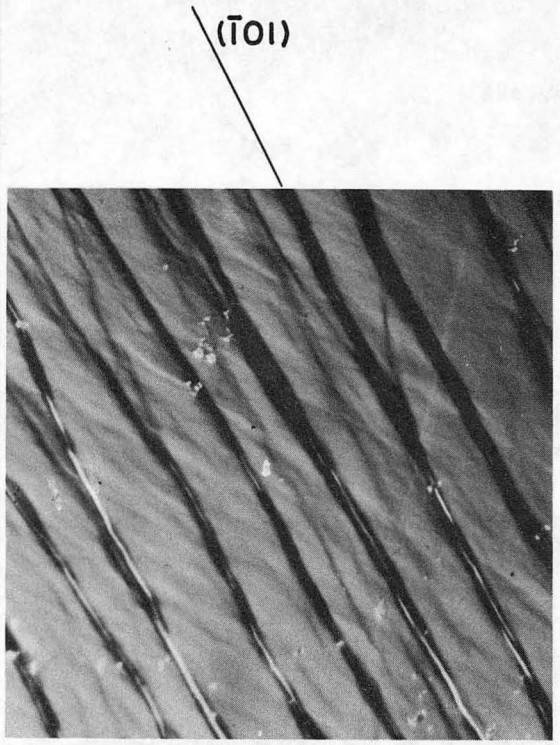

FIG. 13d SLIP TRACES OF SPECIMEN G 1 S
DEFORMED AT 550°K TO 1% ELONGATION.

$X_1' = -4°$ "G"

XBB 694-2477

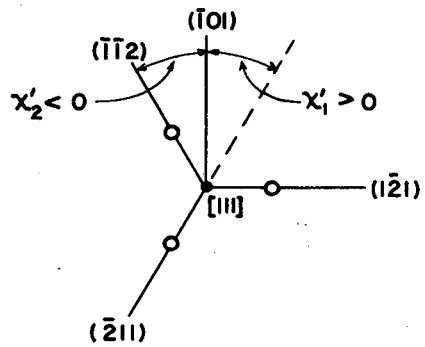

FIG. 14a THE SPLITTING ON THE CORE OF $\frac{a}{2}$ [111] SCREW DISLOCATION.

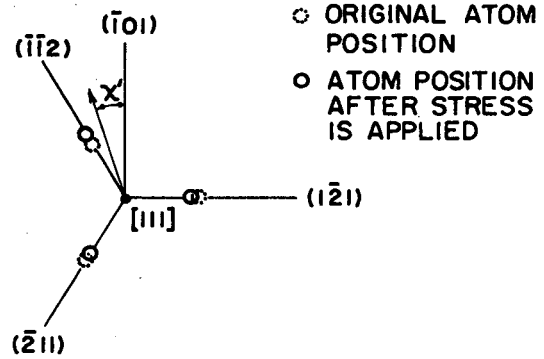

THE ARROW REPRESENTS THE DIRECTION OF THE APPLIED STRESS.

THE CORE SPLITS MORE ON (1̄1̄2) THAN ON (2̄11) AND (12̄1).

FIG. 14b ASYMMETRIC CORE OF THE SAME DISLOCATION.

XBL 694-398

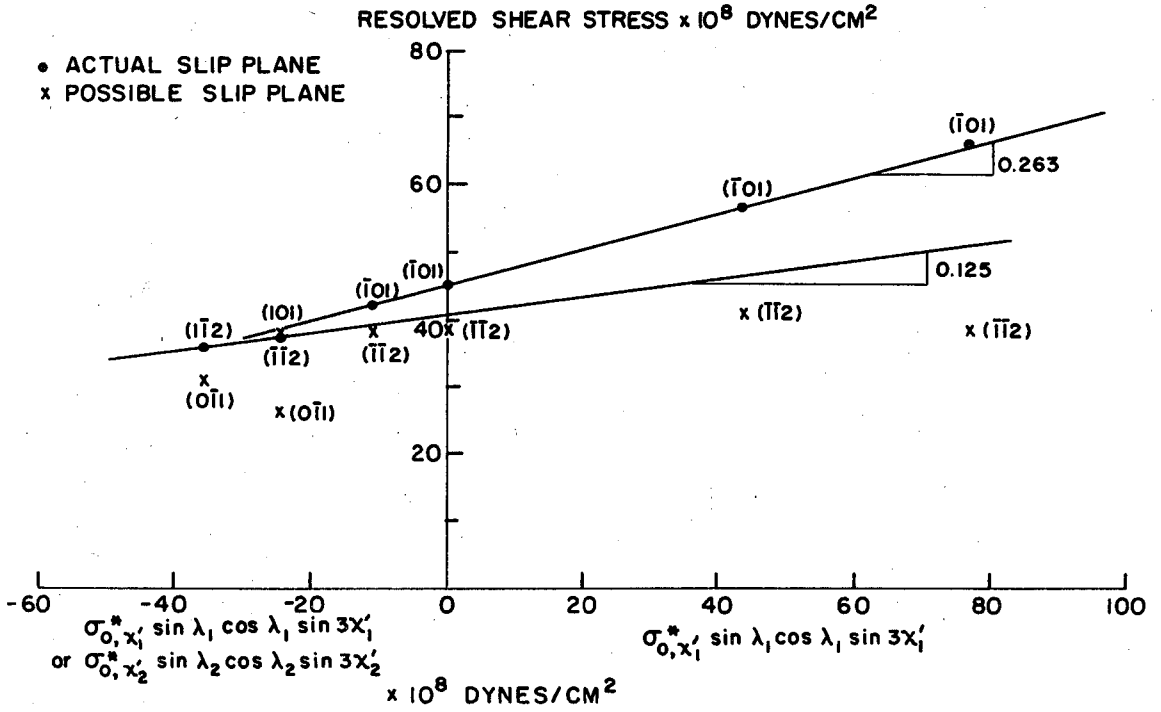

XBL 694-399

FIG. 15

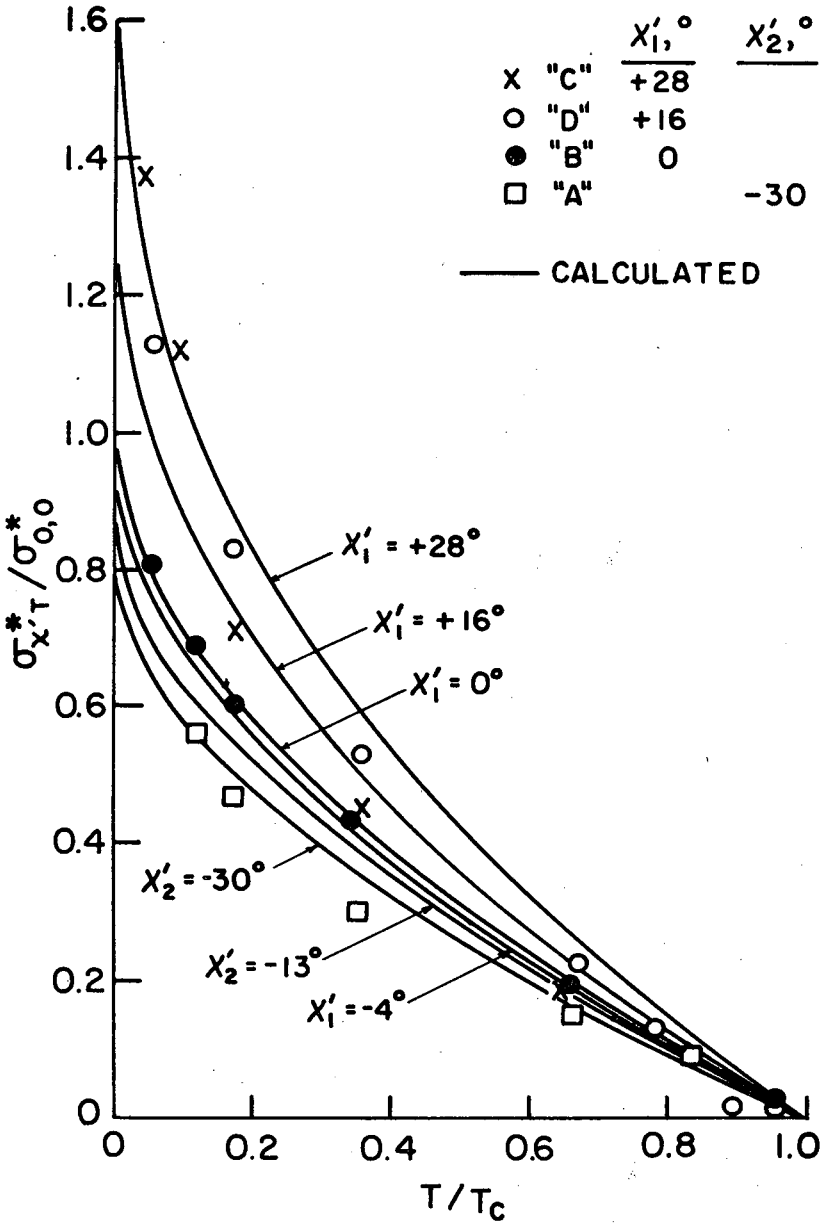

FIG. 16a NORMALIZED YIELD STRESS vs. REDUCED TEMPERATURE.

XBL 694-400

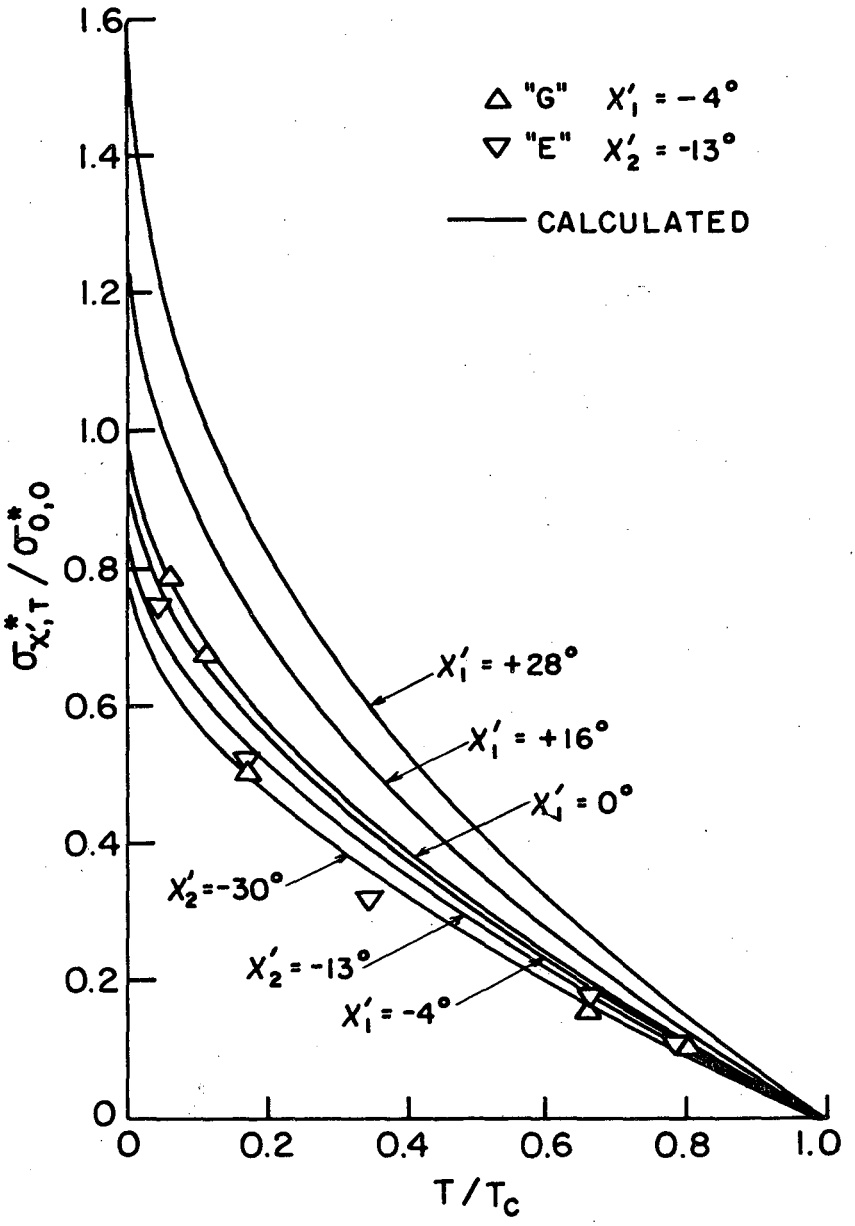

FIG. 16b NORMALIZED YIELD STRESS vs. REDUCED TEMPERATURE.

XBL 694-390

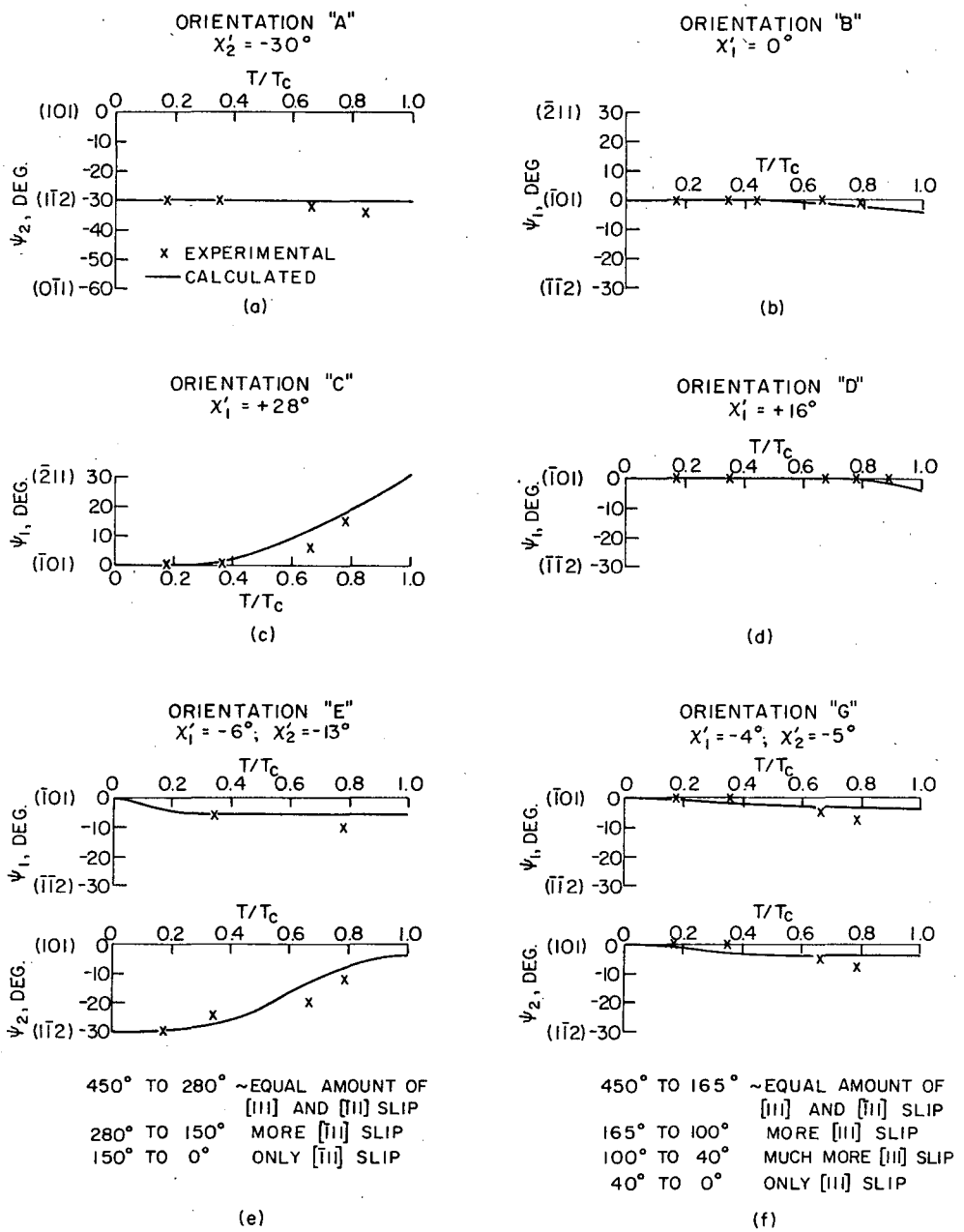

FIG. 17 THE SLIP GEOMETRY.

XBL 694-401

TECHNICAL INFORMATION DIVISION
LAWRENCE RADIATION LABORATORY
UNIVERSITY OF CALIFORNIA
BERKELEY, CALIFORNIA 94720